

Santa Clara University

**Scholar Commons**

---

Mechanical Engineering Senior Theses

Engineering Senior Theses

---

6-14-2023

## **Stabilization Trajectory and Recovery System for High Altitude Weather Balloon Payloads (S.T.A.R.)**

Robert Canalas

Aaron Juan

Miles Nguyen

James Oblitas

Anne Paloma

Follow this and additional works at: [https://scholarcommons.scu.edu/mech\\_senior](https://scholarcommons.scu.edu/mech_senior)



Part of the [Mechanical Engineering Commons](#)

---

**SANTA CLARA UNIVERSITY**

Department of Mechanical Engineering

I HEREBY RECOMMEND THAT THE THESIS PREPARED  
UNDER MY SUPERVISION BY

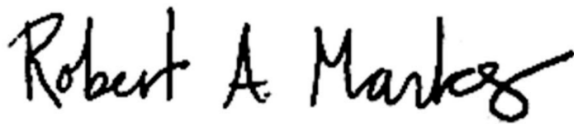
Robert Canalas, Aaron Juan, Miles Nguyen, James Oblitas, Anne Paloma

ENTITLED

**STABILIZATION TRAJECTORY AND RECOVERY SYSTEM FOR  
HIGH-ALTITUDE WEATHER BALLOON PAYLOADS (S.T.A.R.)**

BE ACCEPTED IN PARTIAL FULFILLMENT OF THE REQUIREMENTS  
FOR THE DEGREE OF

**BACHELOR OF SCIENCE**  
IN  
**MECHANICAL ENGINEERING**



June 15, 2023

---

Robert Marks, Thesis Advisor

Date

Hohyun Lee (Jun 16, 2023 09:27 PDT)

06/16/23

---

Hohyun Lee, Department Chair

Date

# STABILIZATION TRAJECTORY AND RECOVERY SYSTEM FOR HIGH-ALTITUDE WEATHER BALLOON PAYLOADS (S.T.A.R.)

By

Robert Canalas, Aaron Juan, Miles Nguyen, James Oblitas, Anne Paloma

## **SENIOR DESIGN PROJECT REPORT**

Submitted to  
the Department of Mechanical Engineering

of

SANTA CLARA UNIVERSITY

in Partial Fulfillment of the Requirements  
for the degree of  
Bachelor of Science in Mechanical Engineering

Santa Clara, California

June 14, 2023

# Stabilization Trajectory and Recovery System for High Altitude Weather Balloon Payloads

(S.T.A.R.)

Robert Canalas, Aaron Juan, Miles Nguyen, James Oblitas, Anne Paloma

Department of Mechanical Engineering

Santa Clara University

2023

## ABSTRACT

Of the 657,000 global balloon launches each year, only 20% of payloads are recovered, leading to unsustainable business and environmental practices. This paper details the development and evaluation of the S.T.A.R. (Stabilization, Trajectory, and Recovery) system, which increases the recovery rate of weather balloon sensors by enabling ideal landing conditions. System testing concludes that S.T.A.R. is capable of housing weather sensors in a fully controllable glider capable of targeted landing. If properly scaled up and redesigned for mass production, the S.T.A.R. system increases weather-sensing equipment recovery for weather-reporting institutions around the world. Although the featured iterations consist of basswood, carbon fiber spars, and 3D-printed parts, future iterations should be made primarily of foam for expedited manufacturing. This additionally allows for a lightweight and uniform cylindrical body to reduce drag.

**Keywords:** Aerodynamics, Atmospheric Data, Glider, Rapid Prototyping, CAD, CFD, 3D-Printing, Sustainability

# Acknowledgements

This thesis, in its research and conclusions in its entirety, are dedicated to our friends and families who have cheered in times of joy and comforted in times of sorrow. Their emotional support is an invaluable asset for the completion of this work.

We would like to extend our sincere gratitude to Joseph Maydell of High Altitude Science, Mike Leggett of Santa Clara County Model Aircraft Skypark, Rodney Broome of Santa Clara University, and our faculty advisor Dr. Robert Marks for assisting us with our project.

# Table of Contents

ABSTRACT.....	iii
Acknowledgements.....	iv
Table of Contents.....	v
Table of Figures.....	vii
List of Tables.....	ix
Nomenclature.....	x
1. Introduction and Background.....	1
1.1. Traditional Weather Balloon Systems.....	1
1.2. Preliminary Market Surveying.....	3
1.2.1. Target Market.....	3
1.2.2. High Altitude Science Survey Questions and Answers.....	4
1.2.3. Design Requirements and Concept Finalization.....	4
1.2.4. Design Challenges and Regulations.....	6
1.3. Value Proposition.....	6
1.4. Ethics.....	6
2. Design and Analysis.....	8
2.1. Initial Sketches.....	8
2.2. Electronics.....	9
2.3. Version 1.....	12
2.3.1. Design.....	12
2.3.2. CFD.....	14
2.3.3. FEA.....	19
2.3.4. Manufacturing Decisions.....	22
2.3.4.1. Bill of Materials.....	22
2.3.4.2. Laser Cutting.....	22
2.3.4.3. 3D Printing.....	25
2.3.5. Construction.....	26
2.3.6. Troubleshooting & Critical Flaw Identification.....	32
2.4. Version 2.....	33
2.4.1. Version 1 to Version 2 Design Changes.....	33
2.4.2. CFD.....	36
2.4.3. FEA.....	42
2.4.3.1. Stress Analysis.....	43
2.4.3.2. Frequency Analysis.....	46
2.4.4. Manufacturing Decisions.....	48

2.4.5. Wing 3D Printing.....	48
2.4.6. Construction.....	52
3. Testing.....	53
3.1. Testing Location.....	53
3.2. Initial Glide Test & Control Surface Trimming.....	53
3.3. Experimental Setup.....	55
3.3.1. Helium.....	55
3.3.2. Connections.....	56
3.3.3. General System and Release Mechanism Test.....	58
3.4. Test 1.....	60
3.5. Test 2.....	63
4. Conclusion & Next Steps.....	65
4.1. Satisfaction of Design Requirements.....	65
4.2. Future Prototype Iterations.....	67
4.2.1. Manufacturing Decisions.....	67
4.2.2. Future Construction Practices.....	68
4.3. Projected Large-Scale Implementation and Mass-Production.....	69
4.3.1. Design Changes.....	69
4.3.2. Expected Cost of Production.....	70
5. References.....	71
6. Appendix A - High Altitude Science Survey Q&A.....	74

# Table of Figures

Figure 1: Labeled Diagram of Current Weather Balloon System [1].....	2
Figure 2: S.T.A.R. Preliminary Conceptual Designs.....	9
Figure 3: Prototype Electronics Setup (a) and Schematic (b).....	11
Figure 4: Version 1 CAD Assembly.....	13
Figure 5: General Airfoil with Nomenclature Terms [7].....	14
Figure 6: SA 7035 Airfoil Lift Curve [8].....	15
Figure 7: Preliminary Analysis of the SA 7035 Airfoil Relative to 1 atm.....	16
Figure 8: (a) Lower and (b) Upper Surface Pressure Gradient Visualization.....	19
Figure 9: Physical Response of Wing to Pressure Gradients (mm of deflection).....	21
Figure 10: Weight Reduction Skeletonization Cuts.....	23
Figure 11: Body Shell and Corner Joints.....	23
Figure 12: Bending the Front Fuselage Parts.....	25
Figure 13: PrusaSlicer with Connector Pieces Oriented Vertically.....	26
Figure 14: Prototype Version 1 Assembly.....	27
Figure 15: Fuselage Servos.....	29
Figure 16: (a) Roll Control Servos and (b) Yaw & Pitch Control Servos.....	29
Figure 17: Tail Control Surface Connections.....	30
Figure 18: Emergency Parachute Release.....	31
Figure 19: Version 1 Actual Center of Gravity (black) vs. Ideal (blue).....	32
Figure 20: Version 1 CAD Assembly.....	34
Figure 21: Version 2 CAD Model.....	34
Figure 22: CAD Drawing of S.T.A.R. Version 2.....	35
Figure 23: (a) Comparison Between Tet Mesh and (b) Poly Mesh.....	37
Figure 24: Coefficient Measurements.....	38
Figure 25: Glide Ratio Visualization.....	39
Figure 26: Wing Bottom Face Pressure Distribution.....	40
Figure 27: Experimental Shedding Frequencies [18].....	42
Figure 28: Visualization of Wing Shedding Frequencies.....	42
Figure 29: (a) Pressure Distributions on the Bottom and (b) Top of the Wings.....	44
Figure 30: (a) Von Mises Contours Along the Top and (b) Bottom of the Wing.....	45
Figure 31: Critical Stress Location.....	46
Figure 32: Resultant Vibrational Amplitudes at the Wing Natural Frequency.....	47
Figure 33: Wing (light blue) with Grid Body (dark blue) with center slot removed.....	50
Figure 34: CAD Result of Wing with Vase Mode Optimizations and Internal Ribs.....	50
Figure 35: Ultimaker Cura Slicer View of Vase Mode Wing.....	51

Figure 36: X-Ray View of Cura Vase Mode Wing Slicing.....	51
Figure 37: Final 3D-Printed Wing Cross Section.....	52
Figure 38: Control Surface Sensitivity Adjustment.....	54
Figure 39: Weather Balloon Inflator Adapter.....	57
Figure 40: Inflated Balloon and Hose Connection.....	57
Figure 41: Balloon Release Mechanism Test.....	59
Figure 42: Initial Release.....	60
Figure 44: Moments Before Skid Landing on Runway.....	62
Figure 45: S.T.A.R. in the Field.....	64
Figure 46: Proposed CAD for Version 3.....	67

# List of Tables

Table 1: S.T.A.R. Design Requirements..... 4  
Table 2: Purchased electronics for S.T.A.R. system..... 10  
Table 3: Bill of Materials..... 22  
Table 4: Version 2 Changelog..... 35  
Table 5: Wing Yield Material Properties..... 43  
Table 6: Modal Frequencies..... 47  
Table 7: Airfield Dimensions [19]..... 53  
Table 8: Parameters for Helium Calculation..... 56  
Table 9: Test Results..... 65

# Nomenclature

Symbol	Description	Units
$a$	Speed of Sound	m/s
$\alpha$	Angle of Attack	degree
$C_d$	Drag Coefficient	–
$C_l$	Lift Coefficient	–
$\delta$	Boundary Layer Thickness	m
$E$	Glide Ratio	–
$h$	Geometric Altitude	m
$g$	Gravitational Acceleration	m/s <sup>2</sup>
$\gamma$	Heat Capacity Ratio	–
$L$	Flat Plate Length	m
$M$	Mach Number	–
$m$	Mass	kg
$\mu$	Dynamic Viscosity	Pa s
$\omega$	Vortex Shedding Frequency	rad/s
$R$	Specific Gas Constant	J/(kg K)
Re	Reynolds Number	–
$\rho$	Density	kg/m <sup>3</sup>
St	Stanton Number	–
$T$	Absolute Temperature	K
$u, v$	Velocity	m/s
$x$	Rectangular Coordinate	m

# 1. Introduction and Background

Weather companies spend millions of dollars each year on sensors to collect atmospheric data for research and general forecasting. Although these sensors allow for real-time data collection, unideal landing conditions cause the vast majority of sensors to never be returned. This not only results in an economic loss for companies but certain components in weather balloon systems can be harmful to the environment. The S.T.A.R. system aims to reduce operational costs while ceasing the careless abandonment of environmentally harmful materials.

## 1.1. Traditional Weather Balloon Systems

Traditional weather balloon systems gather data on the current state of the atmosphere for computers to predict and extrapolate future atmospheric conditions. These systems consist of the following components: a weather balloon, parachute, radiosonde, and a transmitter or communication device as illustrated in Figure 1.

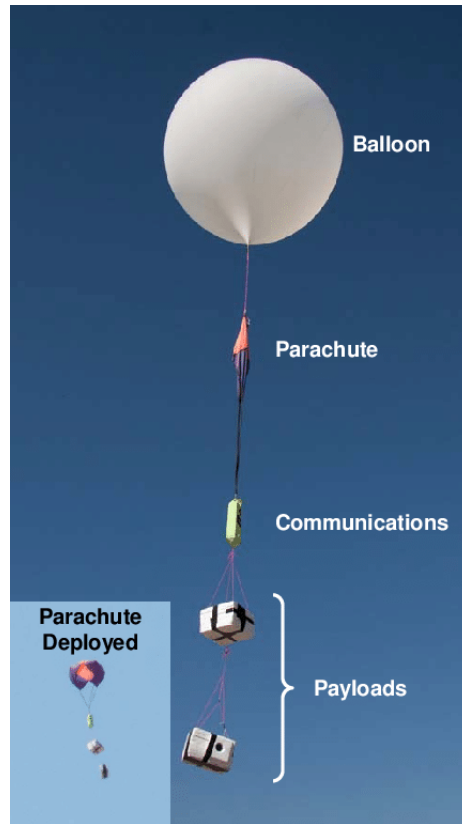


Figure 1: Labeled Diagram of Current Weather Balloon System [1]

Weather prediction and forecasting require sufficient data collection typically achieved by performing two daily weather balloon launches per target area. To satisfy this need, 900 launch locations worldwide allow for 1,800 launches every day, totaling 657,000 launches every year [2]. Radiosondes are the most commonly used weather sensors, typically mounted to weather balloon systems to measure temperature, pressure, and relative humidity. In addition to GPS location, the data collected by this equipment is relayed back to a receiver in real-time through a transmitter connected to the radiosonde.

After tethering and filling weather balloons, they are released into the air with the potential to reach altitudes as high as 100,000 feet. During its ascent, the system can be exposed to harsh storms and temperatures as cold as  $-50^{\circ}$  Fahrenheit [3]. Weather balloon payloads must

be sufficiently resistant to these conditions to ensure proper data collection and transmission. As the system rises, the helium in the balloon expands due to the decreasing atmospheric pressure, causing the balloon to expand and eventually pop. This deploys the payload's parachute, which slows descent back towards the ground. However, the system's landing location is completely determined by the wind, which can result in unfavorable landing locations such as private property, large bodies of water, treetops, and remote locations. This is the primary reason why only 20% of radiosondes released in the United States are recovered [2]. This is an unsustainable practice and results in companies losing millions of dollars every year.

## 1.2 Preliminary Market Surveying

To address the low recovery rates of weather sensing equipment and unsustainable practices of weather balloon expeditions, the S.T.A.R. system must meet a set of design requirements that realistically solve the issues facing real companies. Accomplishing this task requires understanding the overall target market and contacting a company that accurately represents this market. The team interviewed a weather balloon company, High Altitude Science, in order to answer questions on the initial design and to address any issues or potential improvements of the S.T.A.R. system.

### 1.2.1. Target Market

S.T.A.R. allows researchers, meteorologists, weather reporting institutions, and meteorology organizations to reliably recover weather-sensing equipment used for high-altitude expeditions. These institutions view the 80% payload loss as a necessary cost of operation [2]. S.T.A.R. aims to shift this narrative and provide these institutions with a reusable system that reliably returns their weather-sensing equipment.

### 1.2.2. High Altitude Science Survey Questions and Answers

High Altitude Science is a weather balloon kit and supplies company. Their industry knowledge makes them a valuable resource for understanding traditional operations and for providing insight into potential system improvements. The team contacted High Altitude Science to learn more about the weather balloon industry and the application/implementation of the proposed S.T.A.R. system. The survey questions and answers for this conversation can be found in Appendix A.

### 1.2.3. Design Requirements and Concept Finalization

The team's conversation with High Altitude Science led to several design requirements as shown in Table 1.

Table 1: S.T.A.R. Design Requirements

<b>Design Requirements</b>
Yaw, roll, and pitch adjustment to direct glider towards desired landing position
Glide ratio > 1:1
GPS location transmission
Houses GPS, humidity, pressure, and temperature sensors
Sensor data collection
Total mass of 1 kg or less
Reusable & Weather Resistant

### Flight Control

Full control of the S.T.A.R. system is necessary to achieve a 90% recovery rate.

Long-term recovery is not tested within the scope of this project but design decisions are made with this metric in mind.

### Glide Ratio

The glide ratio is defined as the ratio of the amount of horizontal distance traveled per vertical distance dropped. Although a 1:1 glide ratio is lower than most traditional aircraft or gliders, this is set as a baseline considering the S.T.A.R. system's main goal is to land in a safe and recoverable location rather than return to the launch point.

### Equipment Housing & System Weight

The S.T.A.R. system needs to have the capacity to house all sensors internally and successfully gather data while maintaining a total mass of 1 kg or less. This mass standard is chosen based on FAA regulation that weather balloon payloads cannot exceed 6 lbf (2.72 kg) [4]. A system weight of 1 kg is chosen to be conservative and to ensure the S.T.A.R. system poses no weight concerns for a variety of flight missions.

### Sensor Data Collection & GPS Location Transmission

Users must be able to gather data from the system and know S.T.A.R's landing location.

### Reusable

For the S.T.A.R. system to be economically beneficial to companies, the system must be reusable to justify its additional cost and development. Lastly, the previously mentioned low-temperature exposure necessitates weather-resistant housing that minimizes the possibility of a system failure.

#### 1.2.4. Design Challenges and Regulations

The S.T.A.R. system must house electronics (sensors, servo motors, and logic boards) in a small fuselage to minimize overall weight while attaining sufficient lift during descent. Moreover, testing the S.T.A.R. system requires meeting FAA requirements, including (1) restriction of operation to visual line of sight, (2) registration as a drone with the FAA, and (3) prohibition of flight at active airports and FAA-Recognized Identification Areas.

### 1.3. Value Proposition

---

#### Mission Statement

---

S.T.A.R. is a reusable stabilization, trajectory, and recovery system that ensures controlled descent and favorable landing conditions by housing weather balloon sensors within a controllable glider. This allows for more expensive and precise weather-sensing equipment to be used and reliably recovered.

---

Globally, 657,000 weather balloons are launched every year, and only 20% [2] of their payloads (131,400) are ever recovered. With a typical price of \$200, 525,600 radiosondes cost companies \$105,120,000 on an annual basis worldwide. To address this issue, the S.T.A.R. system aims to increase the recovery percentage to 90%, effectively saving companies \$91,980,000 each year when compared to traditional systems. S.T.A.R. demonstrates that profitability and sustainability can not only coexist but be mutually beneficial.

### 1.4. Ethics

Traditional weather balloon systems contain components that are not environmentally friendly and should not be seen as disposable subsystems. Components such as styrofoam,

batteries, printed circuit boards (PCBs), and nylon connection cords are dangerous for wildlife and are pollutants to the environment [5]. Unattended batteries decay and break down over time, causing chemical leakage that contaminates the ground and water systems. This leakage is harmful to the local environment's plants, animals, and even to human populations who inhabit the local area. Styrofoam takes up to 500 years to decay and is dangerous to animals who might otherwise ingest the material [6]. Additionally, nylon cords can wrap around animals' necks and cause death through suffocation or entrapment. Because widespread methods of payload recovery do not currently exist, companies are forced to take on the \$200 operational loss for each launch. The S.T.A.R. system aims to reduce operational costs while ceasing the careless abandonment of harmful materials.

## 2. Design and Analysis

The Design and Analysis of the S.T.A.R. system takes place over a seven-month period. This lengthy process entails two full design iterations followed by a conceptual model for a third iteration. After creating initial sketches, the team begins the design process, after which the electronic specifications, CFD analysis, FEA, manufacturing, and troubleshooting are completed in order to prepare the system for testing.

### 2.1. Initial Sketches

Figure 2 shows the initial sketches of the proposed S.T.A.R. system, which were generated while brainstorming prior to conducting market research. The sketches portray an emergency parachute release, weather sensor attachment areas, and electronics housed throughout the fuselage. These locations are rough estimations and are altered in future iterations.

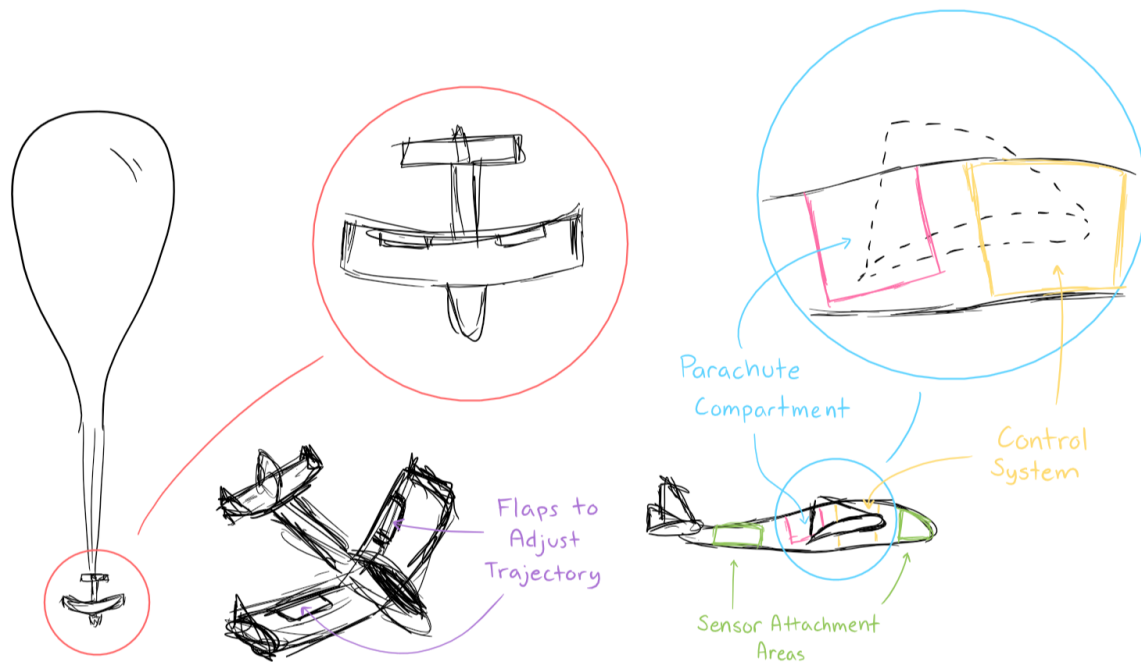


Figure 2: S.T.A.R. Preliminary Conceptual Designs

## 2.2. Electronics

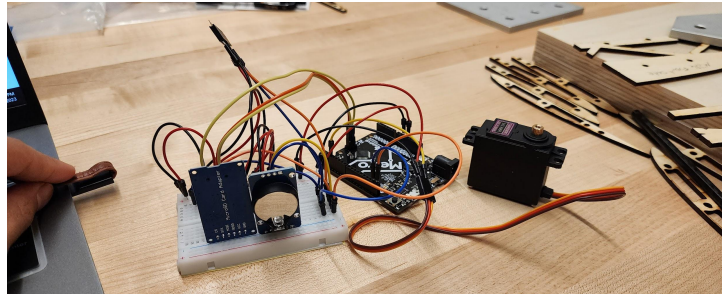
To simulate sensor housing in the final production of the S.T.A.R. system, a set of basic weather sensors are integrated into the body of the glider. These sensors replicate weight and housing locations and will enable verification of the ability to gather data inside the fuselage. Although the final production of the S.T.A.R. system would include an on-board control system, testing will be executed using a commercially available radio transmitter operated by an experienced pilot on the ground. Onboard electronics and other communication devices are shown in Table 2.

Table 2: Purchased electronics for S.T.A.R. system

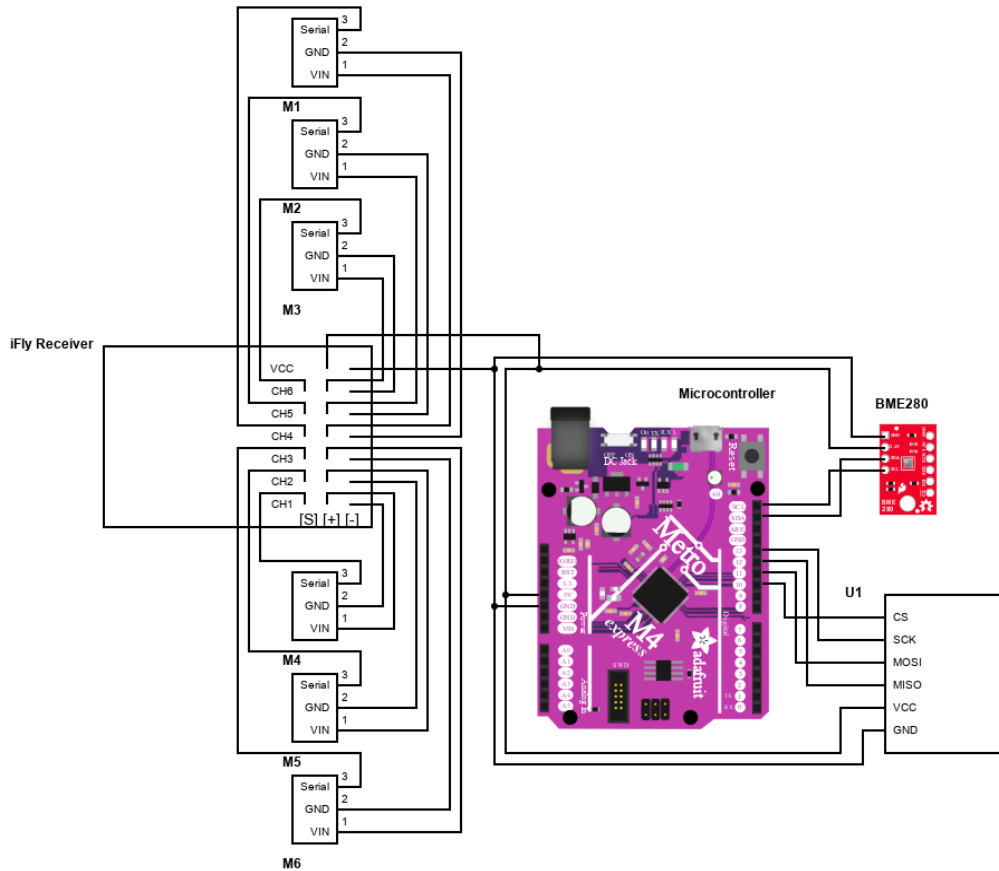
Required Electronic Part	Component Model	Quantity
Temperature, Pressure, and Humidity Sensor	Adafruit BME280	1
RTC Module for Time Keeping	HiLetgo DS3231	1
Accelerometer Gyroscope Module	HiLetgo MPU-6050 6DOF 3-Axis	1
MicroSD Card Adapter	HiLetgo Micro SD TF Card Adapter Reader Module 6Pin	1
Remote Controller & Receiver	Flysky FS-i6 6CH 2.4GHz Radio System RC Transmitter Controller with FS-iA6 Receiver	1
Microcontroller	Adafruit Metro 328	1
GPS Module and Antenna	Dweii GY-NEO6MV2 NEO-6M GPS Module	1
4 AA in Series Battery Box	LAMPVPATH 4 AA Battery Holder	2
Micro Servo	SG90 9g servo	6
Large Servo	MG996R 55g Digital Servo	1
Batteries	NiMH 2000mAh AA Batteries	8
Battery Charger	NiMH AA/AAA Battery Charger	1

All sensors and servo motors are connected to and powered by the Adafruit Metro Microcontroller which is powered by 4 AA batteries (6V). Figure 3a shows an example of the sensors and one test motor. Not pictured is the FlySky RC plane remote controller and transmitter which controls the servo motors attached to the ailerons, elevators, and rudder. Unfortunately, the DS3231, NEO-6M GPS, and MPU-6050 are defective and therefore, they will be excluded from the system. Upon further inspection, the defective electronics were found to be counterfeit products sold on Amazon. The labeling on the devices was incorrect for all of the

pinouts and a few of them couldn't even be powered. Figure 3b shows how all of the working electronics are connected, including the remote RC plane controller.



(a)



(b)

Figure 3: Prototype Electronics Setup (a) and Schematic (b)

## 2.3. Version 1

Using Onshape, a browser-based CAD software, the first version of the S.T.A.R. system is designed to primarily be laser cut. Additional components included 3D-printed PLA and carbon fiber rods.

### 2.3.1. Design

The CAD assembly of S.T.A.R. Version 1 can be seen in Figure 4. This design intends for the majority of the electronics to be mounted in the nose of the glider except the control surface servo motors and emergency parachute servo motors. The control surfaces and emergency parachute release mechanism are covered in Section 2.3.5.

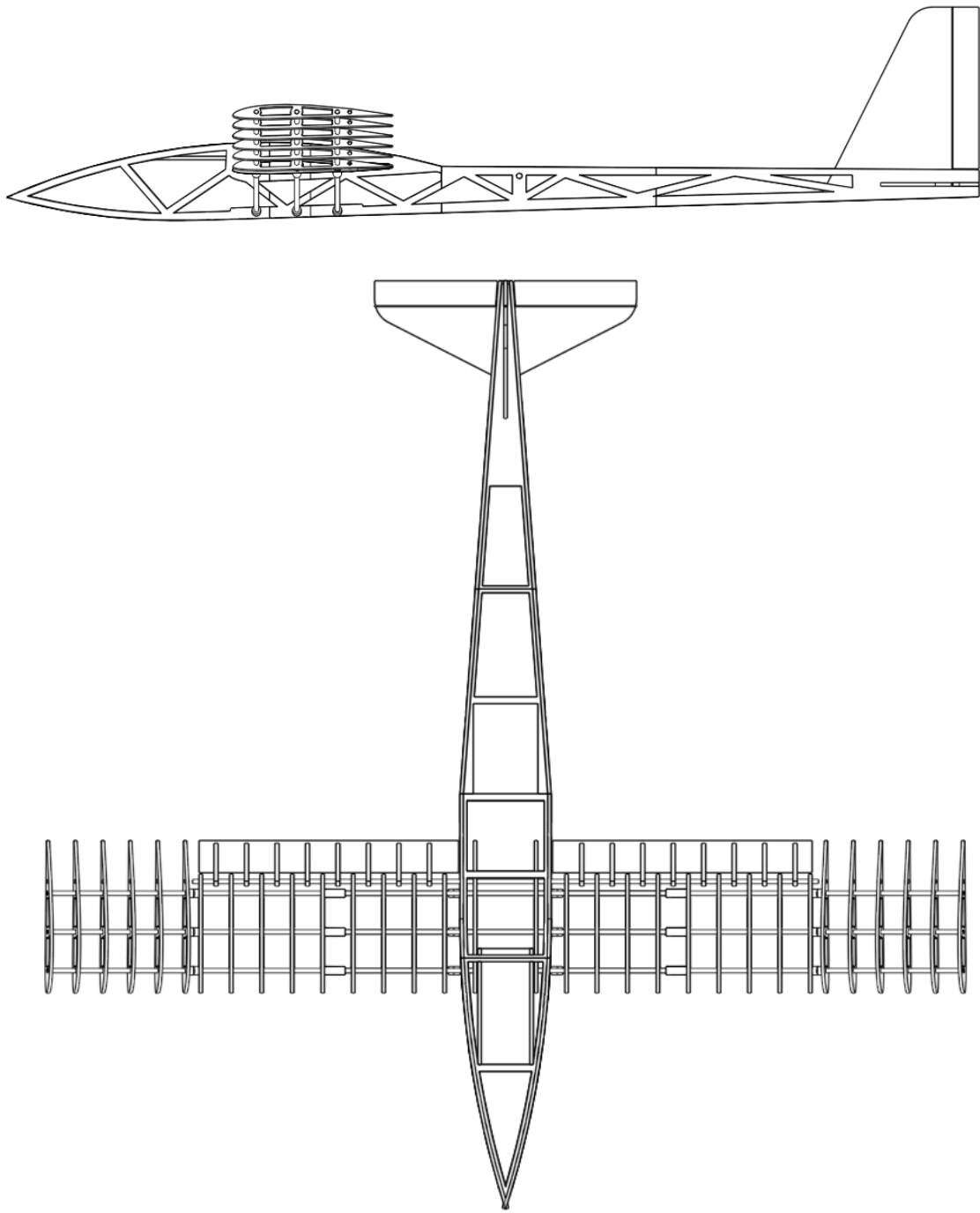


Figure 4: Version 1 CAD Assembly

### 2.3.2. CFD

Multiple types of airfoils exist to promote laminar airflow to reduce the skin friction drag and generate pressure gradients necessary for creating lift. An airfoil is a section of the wing created by the longitudinal and vertical axes of the fuselage and extended in the direction of the lateral axis. For reference, a diagram of a general airfoil is shown in Figure 5.

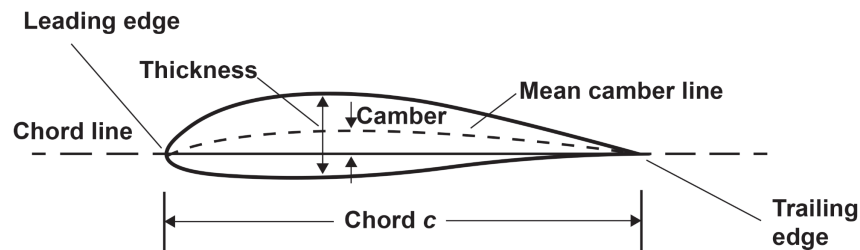


Figure 5: General Airfoil with Nomenclature Terms [7]

All iterations of S.T.A.R. use the SA 7035 airfoil, which is a derivative of a commonly used glider airfoil [8]. The dimensionless coefficients  $C_l$  and  $C_d$  characterize the lift and drag of the airfoil respectively. Furthermore, varying the orientation of the airfoil by changing the angle of attack leads to changes in the lift and drag forces, which thus leads to changes in the lift and drag coefficients. When plotting the lift coefficient versus the angle of attack  $\alpha$ , a generally linear slope is observed. Figure 6 shows the lift-line curve for the SA 7035.

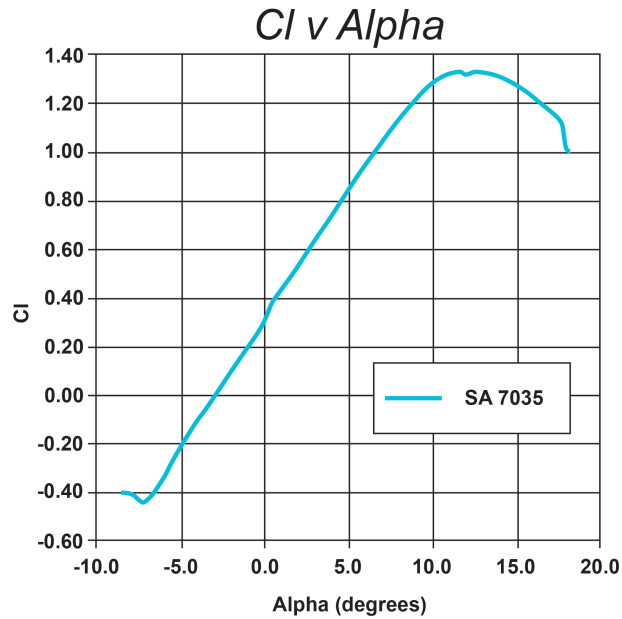


Figure 6: SA 7035 Airfoil Lift Curve [8]

For the purposes of simulation, airfoils are commonly assumed to extend infinitely in the lateral direction; this enables a two-dimensional analysis of the flow properties. While this approximation tends to overestimate the lift coefficient since the flow will typically be different near the ends of the wingspan and fuselage, it is generally considered acceptable provided the wingspan is sufficiently large. To verify the generation of lift, a CFD simulation using Siemens STAR-CCM+ (name purely coincidental) is performed on a solid model of the SA 7035, which is shown in Figure 7.

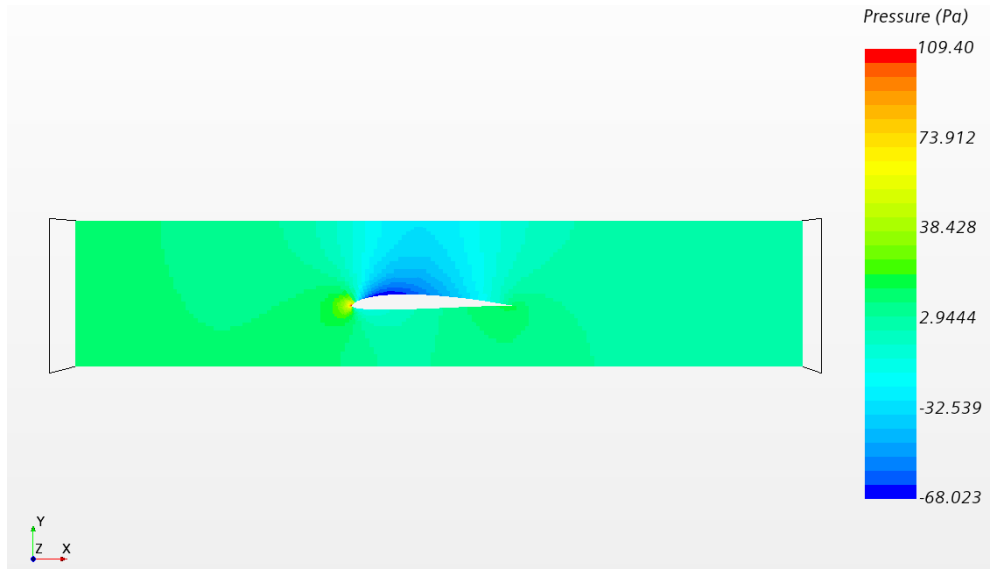


Figure 7: Preliminary Analysis of the SA 7035 Airfoil Relative to 1 atm

The pressure gradient develops from the flow encountering the body, which can only arise from the movement of the surrounding air or the body. It is assumed that one hundred feet or 30.5 meters of elevation drop will be required for S.T.A.R. to pull out of the vertical dive. This speed of the body in still air is equivalent to the speed of the air against a still body. To find the freestream velocity, the velocity of the air far away from the body, one can estimate using a simple conservation of energy calculation as shown in Equation 1.

$$mg\Delta h = \frac{1}{2}mv^2 \quad (1)$$

Here,  $m$  is the mass of S.T.A.R.,  $g$  is the Earth's gravitational constant of  $9.8 \text{ m/s}^2$ ,  $h$  is the geometric altitude of S.T.A.R., and  $v$  is the velocity. Solving Equation 1 for velocity leads to a speed of  $v = 24.442 \text{ m/s}$  regardless of mass. However, this freestream calculation neglects the effects of drag, so a value of  $22 \text{ m/s}$  is instead used. This input velocity is utilized by STAR-CCM+ for simulation purposes.

To conduct the calculations, several assumptions are made to best mimic the flight conditions that S.T.A.R. will fly in. These same assumptions are used in all future iterations. The simulation assumes a steady-state, incompressible flow and obeys k- $\epsilon$  turbulence and segregated regime. All the fluid properties have a temperature, static pressure, and density of 288.16 K, 101.3 kPa, and 1.225 kg/m<sup>3</sup> respectively, which is the standard atmosphere at sea level [9].

STAR-CCM+ offers two types of turbulence models: k- $\epsilon$  and k- $\omega$ . The k- $\omega$  model is known for its higher accuracy for the viscous boundary layer against walled surfaces and internal flows [10]. However, k- $\omega$  has poor convergence rates, which potentially means that the software may not reach a solution [10]. Furthermore, S.T.A.R. does not have internal flows but is a body operating in immersed flow. In contrast, k- $\epsilon$  has a much higher convergence rate and retains high accuracy in complicated geometries. Therefore as a “good general-purpose model,” k- $\epsilon$  was chosen to model the turbulent flow [10]. After selecting a turbulence model, the solver uses either a segregated or coupled flow regime. The coupled solver collectively determines all the properties of state such as momentum and energy together, while the segregated solver calculates those values sequentially [11]. Solving for the properties of state simultaneously leads to improved accuracy against shock density changes such as supersonic flows, but it requires more computation time. As a rule of thumb, flow should be treated as compressible above a Mach number of 0.3, which is a non-dimensionalized quantity to characterize how close the freestream velocity is to the speed of sound [12]. Equations 2 and 3 provide the speed of sound and the Mach number respectively [13].

$$a = \sqrt{\gamma RT} \quad (2)$$

$$M = \frac{u}{a} \quad (3)$$

Here,  $\gamma$  is the heat capacity ratio (1.4 for air),  $R$  is the specific gas constant (287 J/(kg K) for air), and  $T$  is the absolute temperature (288.16 K at sea level), and  $u$  is the freestream velocity [14].

From Equations 2 and 3, the speed of sound at sea level is 340 m/s, which corresponds to S.T.A.R. operating at a Mach number of 0.06, which is significantly less than 0.3. Therefore, the assumption of constant density and segregated flow is valid, and will not have a detrimental effect on the solution.

In reality, all aircraft and glider wings are finite, three-dimensional bodies. There is a limiting value on how far the span of the wing will reach. In doing so, this means that there is space for the high-pressure air in the bottom of the wing to leak upward into the lower-pressure air at the top of the wing, causing trailing vortices at the wingtips. The vortices have a velocity component in the downward direction, which leads to an element of lift acting in the direction of the freestream velocity and inducing drag [14]. The infinite 2D airfoil has a better performance than the 3D finite wing, so it cannot be taken for granted that the properties of the airfoil match the wing. In addition, further additions from mounting the wing to the fuselage lead to a greater cross-sectional area viewed by the freestream velocity, and thus higher drag. Using the concepts stated above, CFD analysis was performed on S.T.A.R. V1.

As shown in Figure 8, the desired pressure gradient develops along the wing. In the particular scenario shown in Figure 8, a lift force of 16.076 N is imposed onto the airframe at a chosen angle of attack  $\alpha = 6^\circ$ . This leads to a factor of safety of 1.632 against the weight of the glider. Using the given dimensions, the aspect ratio AR which is the ratio of the square of the wingspan to the projected planform area is found to be 4.378. Using the lift and drag forces, the

glide ratio  $E$  is calculated to be 2.05. One statistic to note is that the center of pressure  $x_{cp}$  is found to be at approximately mid-chord, which leads to potentially unstable moments being generated onto the airframe. Typical airfoils estimate the center of pressure to be at quarter-chord, which is equivalent to the aerodynamic center [15]. However, this just requires the center of gravity of the airframe to be at the same point as  $x_{cp}$  to maintain stability to counteract the generated moment. Therefore, the glider geometry is sufficient to produce the necessary lift required to maintain flight.

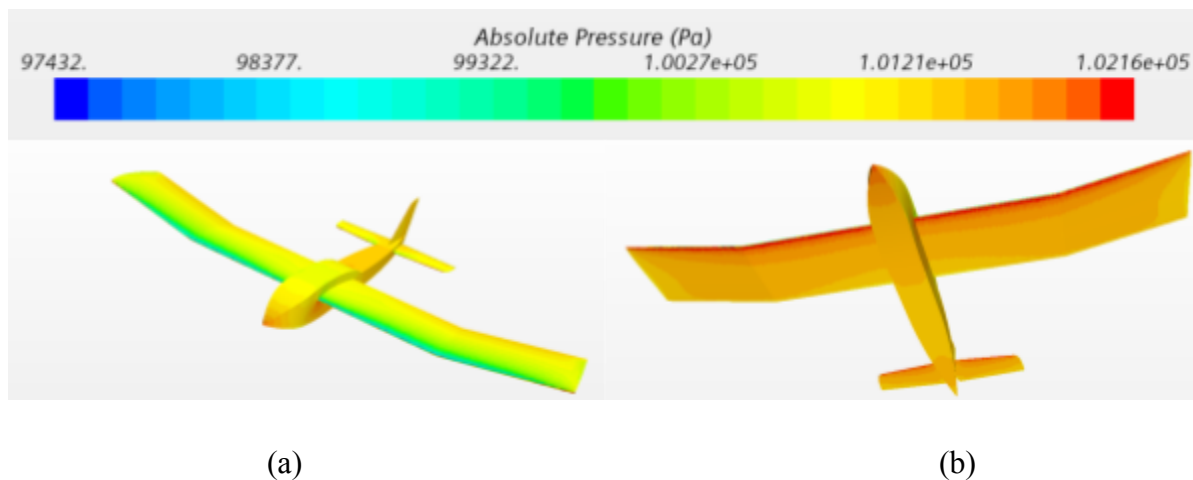


Figure 8: (a) Lower and (b) Upper Surface Pressure Gradient Visualization

### 2.3.3. FEA

After drafting the first wing design, the wing's structural integrity needs to be evaluated in order to ensure that the glider can withstand the forces the environment will exert. Since this is just a preliminary design, the main concern is whether or not the chosen design and materials will excessively bend during flight. Too much upward bending of the wings will affect the flight of the plane, and this study will determine if extra supports are needed. Based on the numbers obtained from the CFD, the FEA can provide deflections at each part of the wing. The deflection study will demonstrate the worst-case performance of the wing. Bending in the wing is normal

for gliders or any model aircraft, but excessive bending can affect the performance of the control system of the glider. The deflection study can help determine if extra support structures must be placed on the wing.

To run the simulations, a few assumptions have to be made in order to properly set up the study in SolidWorks. To make the study simple, a static study is used to capture the worst possible scenario when a pressure distribution is applied across the entire wing. Because the wings will be wrapped in solar film, the pressure distribution will be directly applied to the wood spars and not onto the carbon fiber rods. During the flight, air will go around the solar film, applying the pressure to the wing surface, but the spars will be bearing most of that force, so it is assumed here that the pressure is being acted on the wooden spars. To speed up calculations, the wing is assumed to have the same pressure distribution along the entire span of the wing. Since the primary concern is the performance of the wings, the rest of the glider is also left out of the study to reduce computing time. The wing is just assumed to be fixed at the center where the wing will be attached inside the fuselage.

Before running the simulation, a medium to coarse mesh is applied to the wings. A coarse mesh is applied to maintain the short computation time, but also because the stress gradients are not anticipated to be very high. In addition, the mesh size automatically is set very low by the software because the dimensions of the individual parts are also very small. Upon running the simulation, a deflection graph displays an asymmetric deflection on the wings. The difference, as seen in Figure 9, is about 1.13 mm. Given this strange result, the simulation is run a few more times with finer meshes while also checking that the other parameters are input correctly. The result is consistent across runs and is minute enough to not be noticed by the naked eye when built. Because of this, the simulation is accepted as is. This study still demonstrates key features

necessary for the wings. For such a small wing, the deflection shows that extra support would be needed to prevent excess wing bending. If the flight conditions are worse than expected, then the wings may deflect more than the study shows, therefore support beams need to be placed underneath the wing to pull the wings down.

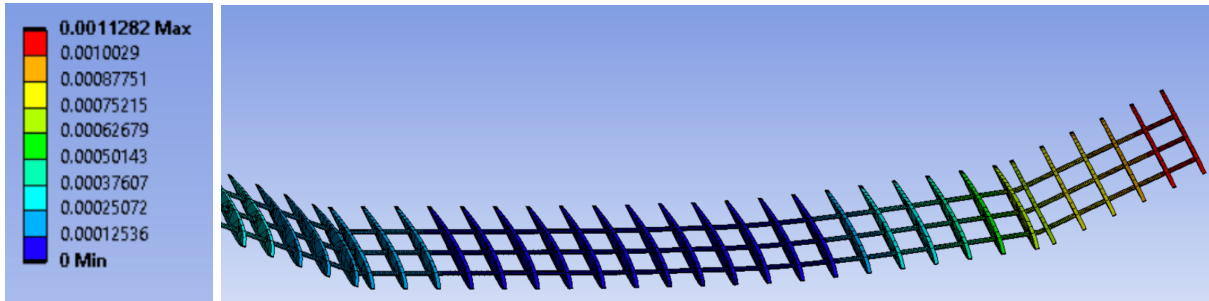


Figure 9: Physical Response of Wing to Pressure Gradients (mm of deflection)

#### 2.3.4. Manufacturing Decisions

The creation of S.T.A.R. V1 combines manufacturing techniques to ensure a strong but lightweight fuselage to ensure a decent factor of safety for lift.

##### 2.3.4.1. Bill of Materials

The bill of materials is shown below in Table 3.

Table 3: Bill of Materials

<b>Component</b>	<b>Quantity</b>
1/8th inch thick laminated Basswood Sheets	2 packs
eSun PLA+ 1.75mm 3D printer filament	1 kg
4mmx420mm Carbon Fiber Rods	20
UltraCote Solar Film Airplane Covering	2 rolls
36-inch Ripstop Nylon Cloth Parachute	1
.039” Music Wire	1 pack
Super Glue	9 tubes
Titebond II wood glue	1
MG996R 55g Digital Servo	1
600 gram Weather Balloon	1
14.9 cubic feet Helium Tank	8

##### 2.3.4.2. Laser Cutting

The Version 1 gilder parts are designed for laser cutting out of 1/8th inch material on a CO<sub>2</sub> Epilog laser cutter. This is achieved by ensuring the fuselage is mostly made of flat panels with some adequately large outer surface radii when required. In order to reduce the overall weight of the fuselage, large panels are removed from the panels, as illustrated in Figure 10.

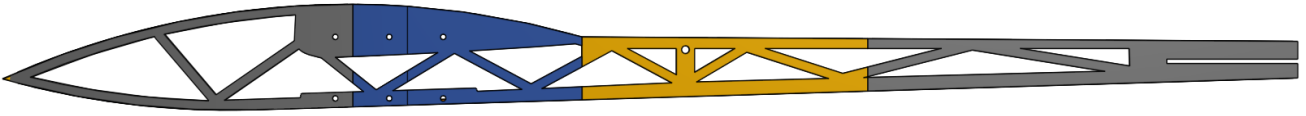


Figure 10: Weight Reduction Skeletonization Cuts.

The solid model is then shelled to an 1/8th inch thickness to be consistent with the proposed material thickness. The shelled CAD model is split so that each of the four faces of the fuselage is a separate part with no interference between them. This result is shown in Figure 11 where the corners touch, but do not intersect. For the sake of simplicity, tongue-in-groove joints are not used, but this is a possible mechanism to increase the strength of the connections between the laser-cut fuselage panels.

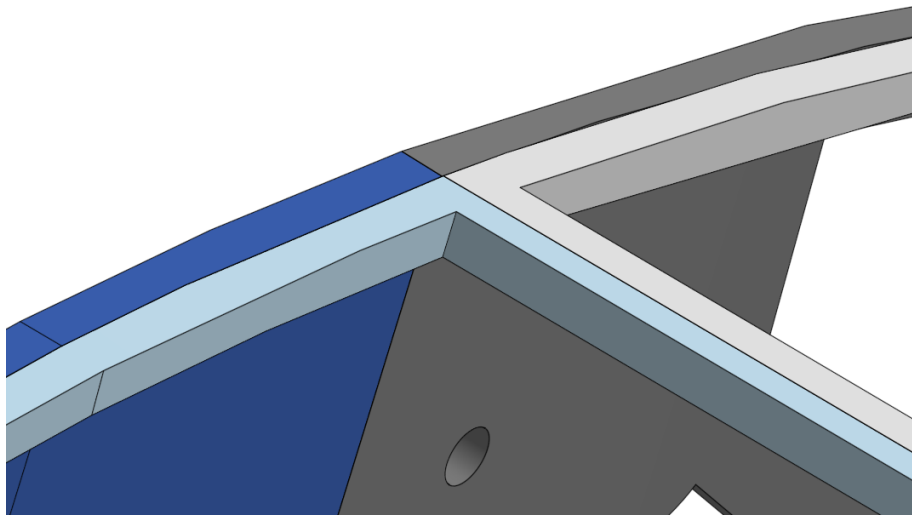


Figure 11: Body Shell and Corner Joints

The outer solid bodies are then converted into surfaces by deleting all the faces except the outermost face of each part, using the “Leave Open” option in the “Delete Faces” tool in Onshape. The remaining faces are then converted into sheet metal parts with a 1/8th inch

thickness using the “Sheet Metal Model” tool. By converting to a sheet metal model, the parts can be flattened, which is necessary because the laser cutter can only cut flat materials. Once flattened, the surfaces can be exported as .dwg or .dxf files. The files are imported into CorelDraw, sent to the Epilog Dashboard, and then cut out of 1/8th inch basswood. Alternatively, Inkscape can be used in place of CorelDraw. Basswood is chosen for the initial design because of the extra strength it would give the fuselage compared to the more commonly used balsa wood. Leaving the cut parts out overnight without ensuring they stay flat results in the parts warping due to the water content in the wood. This renders quite a few of the pieces unusable after being cut, which means extra parts have to be cut to account for the high failure rate.

In order to account for the kerf of the laser, multiple test cuts are performed to determine which hole size would create the best press fit for the carbon fiber wing spars. This test has to be performed twice due to necessary refocusing. After refocusing, the kerf is 0.006” which yields a quality slip fit between the wood and the carbon fiber rods. After cutting the wood, the curved sections of the fuselage need to be bent into their final shapes. These pieces are intentionally soaked in water and allowed to dry with weights pressing down on the center in the orientation shown in Figure 12.

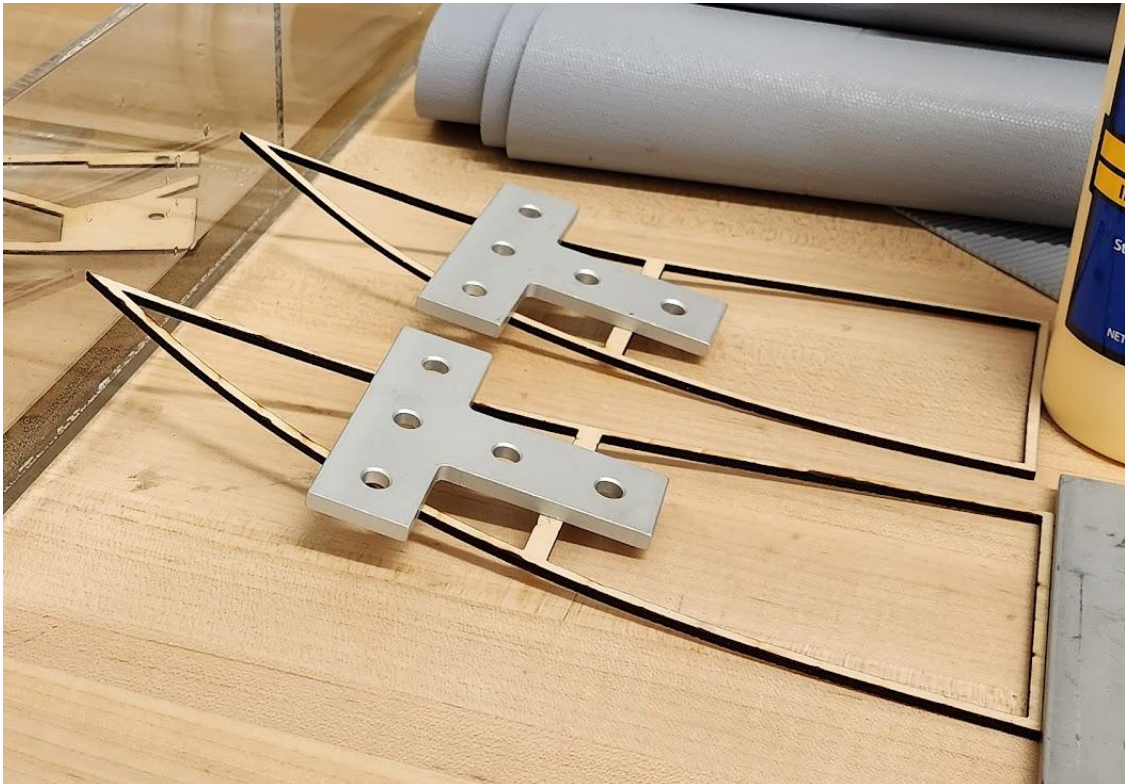


Figure 12: Bending the Front Fuselage Parts

#### 2.3.4.3. 3D Printing

Various miscellaneous connections require sleeves to be slipped over carbon fiber rods in order to connect them to the fuselage or other carbon fiber rods. These sleeves are FDM 3D-printed out of eSun PLA+ in black on a Prusa Mk3 i3 cartesian 3D printer. The connectors are printed vertically as shown in Figure 13 so that the amount of support material generated was minimal. This means that the connectors have to be designed to prevent overhangs greater than 45°. The tolerance/kerf of the printed ID holes is 0.3 mm over the desired ID. The CAD files are sliced in PrusaSlicer 2.5.0 and Ultimaker Cura 4.8.0 interchangeably. The downside of orienting the parts with the through holes perpendicular to the build surface is the need to include a “brim” in the slicers to prevent the parts from detaching while the print is ongoing. However, the brim connects small parts together and makes removal from the bed more efficient.

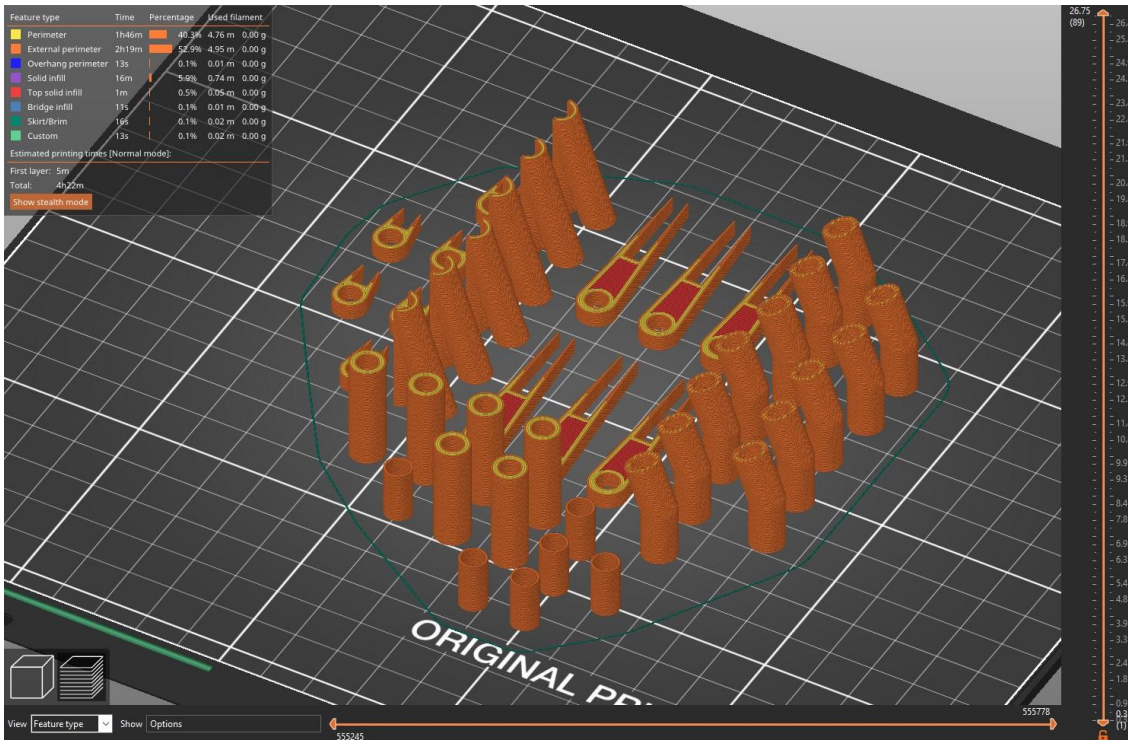


Figure 13: PrusaSlicer with Connector Pieces Oriented Vertically

The use of 3D-printed connectors is kept to a minimum to reduce weight since PLA+ has a higher density than basswood. The print has a 20% infill and two walls with a 0.4 mm nozzle. This makes them lighter than a completely solid part, but the minimum of two walls was an immutable factor that had to be considered. Post-processing of the prints is fairly simple as only the removal of the brim and deburring are required.

### 2.3.5. Construction

Figure 14 shows the Version 1 assembly of S.T.A.R. without the solar film wrapping the fuselage (so interior components can be seen). The fuselage is assembled using Titebond II wood glue for the basswood-to-basswood interfaces. The laser-cut parts that have been soaked and bent are then dried fully to limit the amount of excess moisture in the wood. Blue painter's tape is then used to hold the thin 1/8th inch sections together until the wood glue is set after which the

tape could be removed. For the wood-to-carbon fiber and carbon fiber to PLA+ attachments, cyanoacrylate (superglue) is used. In most cases, the superglue is able to quickly cure anaerobically, but if there is a large pool of glue that is exposed to air, a small amount of baking soda is sprinkled into the superglue which greatly reduces the cure time. Wood glue and superglue are used to secure the cardstock intermediate skin to the wing cross sections. Wood glue is used if cure time is not a limiting factor and the surfaces could be clamped together overnight. Superglue is used when clamping is difficult or when there is limited time available for curing.



Figure 14: Prototype Version 1 Assembly

In order to create a smooth outer surface, a white polyester-based film, or solar film, is wrapped over the fuselage and intermediate cardstock skin. This film is able to bridge small weight-reduction gaps in the fuselage and adhere to the wood and paper by utilizing a heat gun and iron. The film contracts slightly when heated, so pieces have to be cut larger than the fuselage sections, but the end result is a taught uniform surface. Using superglue to attach any materials to this film is difficult because the film does not absorb the glue as the wood does, and the film has the potential to pull away from the fuselage or wings, taking the glued part with it. In order to remedy this problem, small sections of the film are removed any time materials needed to be glued to the fuselage or wings.

The yaw, pitch, and roll control servos are superglued within the fuselage as seen in Figures 15 and Figures 16. The carbon fiber rod of each wing roll control surface is super glued to the black 3D-printed connector that is super glued to each servo shaft. Both the vertical stabilizer flap and horizontal stabilizer flaps are connected to the servos by high carbon steel music wire looped through the holes of servo arms, which are super glued to the ends of the control surface carbon fiber rods as seen in Figure 17. Since the two control surfaces on the horizontal stabilizer rotate around two different carbon fiber rods, as seen in Figure 17, the servo arm connected to the left control surface points upwards while the servo arm connected to the right control surface points downward. This reversed connection allows both surfaces to move in unison and be controlled by a single servo which is the rightmost servo in Figure 16b.

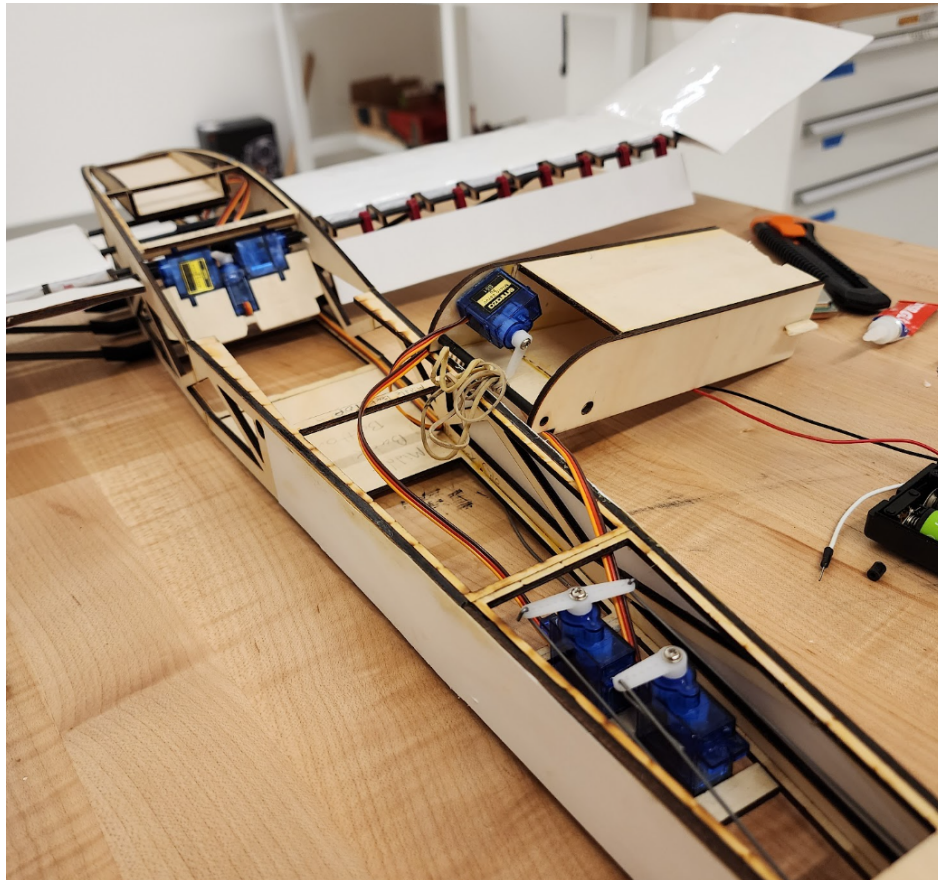
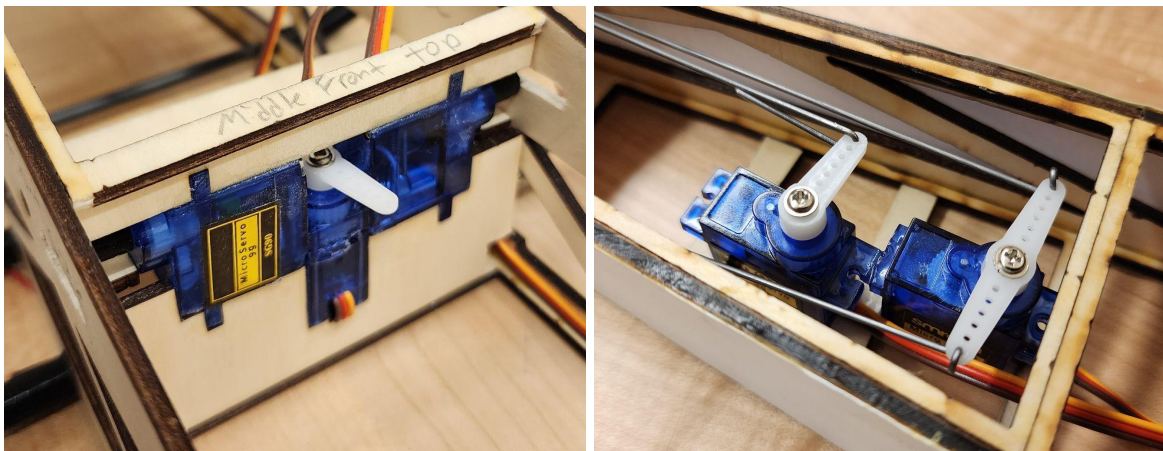


Figure 15: Fuselage Servos



(a)

(b)

Figure 16: (a) Roll Control Servos and (b) Yaw & Pitch Control Servos

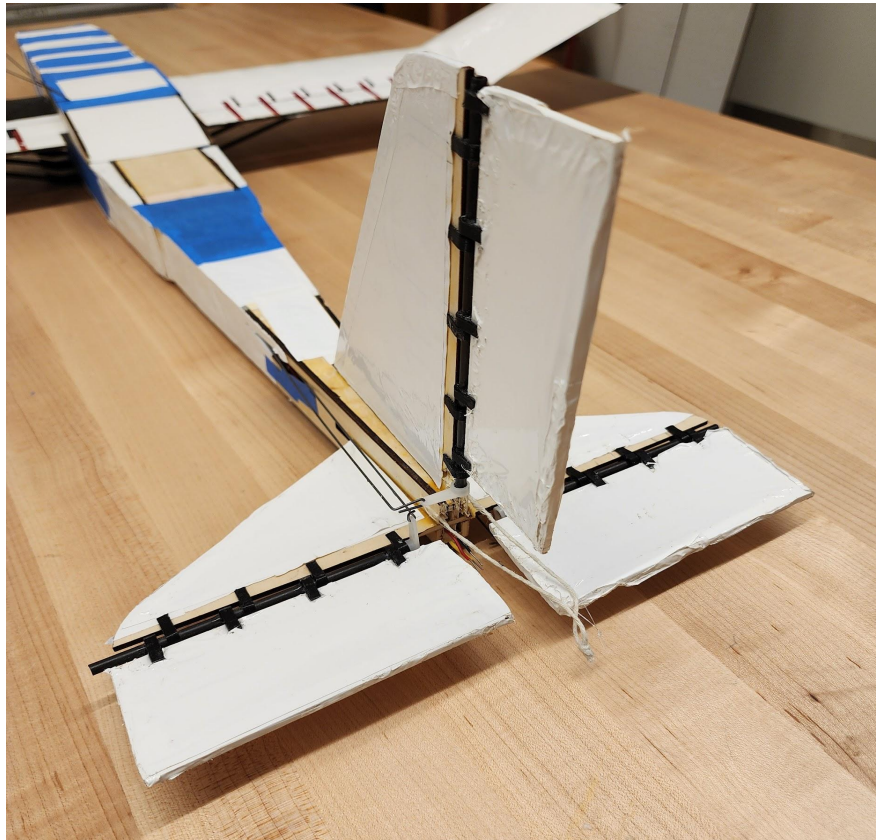


Figure 17: Tail Control Surface Connections

The emergency parachute release has two carbon fiber rods; the first 0.25-inch rod acts as the axis of rotation of the release system, and the second 4mm rod acts as the connection point for the release rubber bands, which provide the tension required for the release system to swing open. The release rubber bands are connected to this second carbon fiber rod on one side and connected to the carbon fiber rods below the wing on the other side. The release system is locked in place by the center release servo in Figure 16a. The small slit both in the release system and ejection system allows them both to rotate past the release servo arm when it is in that position. The parachute is held in place by an ejection servo mounted within the back of the release system. When loading the parachute, it is precisely folded to fit within the ejection housing, which has green ejection rubber bands seen in Figure 18 that is held in place on the exterior of

the release system; this ejection system is held in place by a metal loop that is set up around the ejection servo. When the parachute is deployed during descent, the following servo rotations release and eject the parachute: the release servo arm rotates in order to align with the slit in the release and ejection system, allowing the release system to rotate open due to the tension in the release rubber bands; then the ejection servo rotates, thus unhooking from the metal loop that was locking the ejection system, allowing the ejection rubber bands to force the ejection housing out of the release housing, shooting the parachute out of the glider. The complete Version 1 assembly can be seen in Figure 14.



Figure 18: Emergency Parachute Release

### 2.3.6. Troubleshooting & Critical Flaw Identification

The components are mounted within the fuselage and the center of gravity of the glider is found to be behind the leading edge of the wing, illustrated by the black symbol in Figure 19. Ideally, the center of gravity is located at about a quarter of the cord length behind the leading edge of the wing shown in Figure 19 as the blue symbol. Our test pilot Mike Leggett, from SCCMAS, also recommended that the wingspan of the glider should be increased in order to generate a favorable amount of lift. Along with these considerations, we also needed to reduce the weight. There were many sections of the fuselage that were excessively reinforced; some sections are solid basswood, but the desired structural and geometric properties could be achieved by substituting these solid basswood sections with solar film wrap.

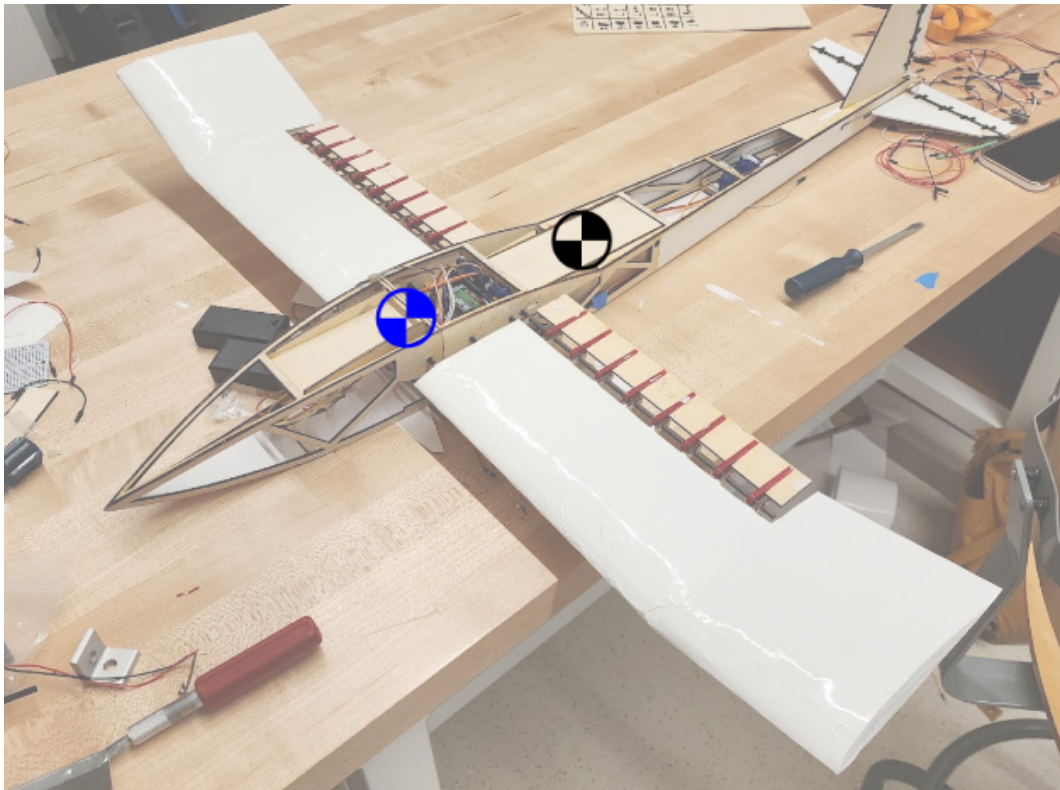


Figure 19: Version 1 Actual Center of Gravity (black) vs. Ideal (blue)

## 2.4. Version 2

Version 2 of the S.T.A.R. system addresses unfavorable center of gravity as well as structural flaws from Version 1. The new version will be simulated and tested against the worst-case scenario flight conditions in order to ensure that the updated design can withstand critical conditions during a flight. After passing all simulated tests, the second version of S.T.A.R. is manufactured and prepared for testing.

### 2.4.1. Version 1 to Version 2 Design Changes

The design changes from Version 1 (Figure 20) to Version 2 (Figure 21) include a larger wingspan made with 3D printing as opposed to laser cutting, the center of gravity moved closer to the nose of the glider which mandated a shortening of the tail and a lengthening of the nose, and general weight reduction all around the fuselage and flaps. A CAD model of Version 2 can be seen in Figure 22. A list of the desired outcomes from these changes and what is done to achieve these goals is listed in Table 4. For reference, Figure 22 shows the dimensions of the length, width, and height of S.T.A.R. V2.

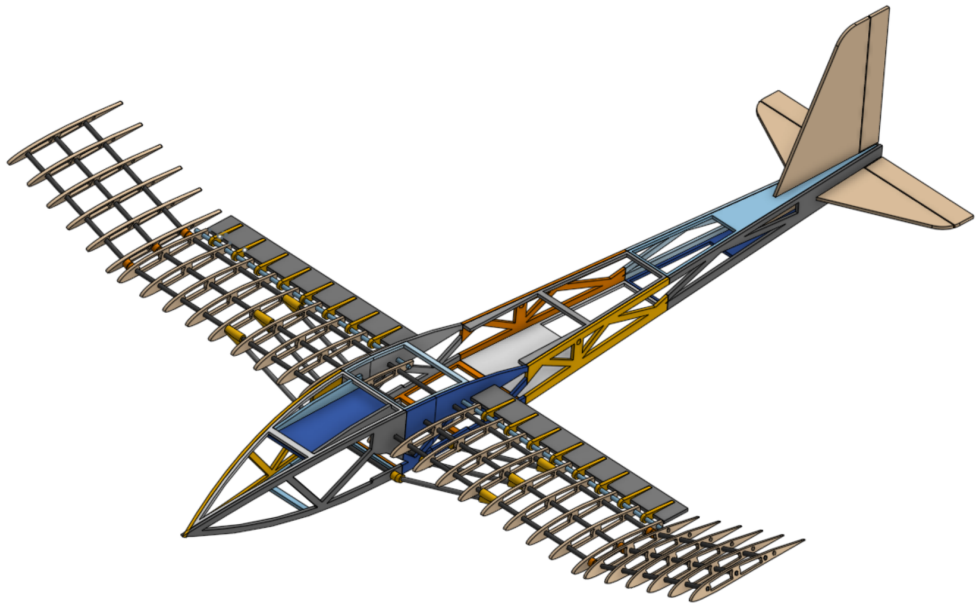


Figure 20: Version 1 CAD Assembly

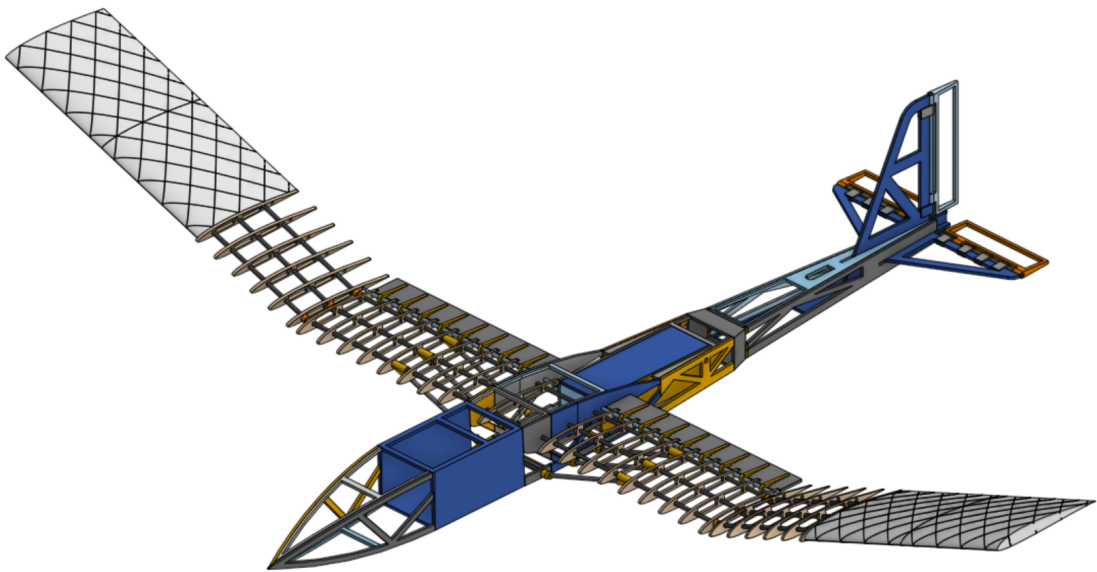


Figure 21: Version 2 CAD Model

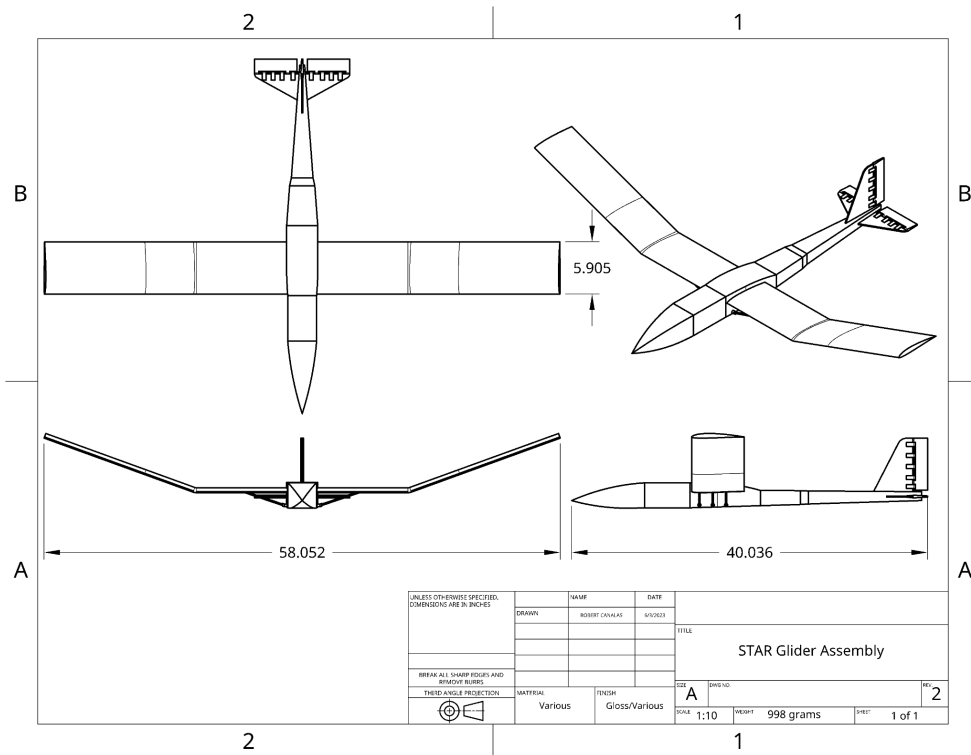


Figure 22: CAD Drawing of S.T.A.R. Version 2

Table 4: Version 2 Changelog

Redesign Objective	Changes Made
Move CG to Quarter-Chord	<ul style="list-style-type: none"> <li>• Add 5-inch long section to the fuselage in front of the wing</li> <li>• Remove 3.5-inch long section from the fuselage behind the wing</li> <li>• Make skeletonization cutouts behind the wing where possible without compromising structural integrity</li> <li>• Mount batteries and electronics as close to the nose as possible</li> </ul>
Increase Lift Force	<ul style="list-style-type: none"> <li>• Increase skeletonization mentioned above to decrease total system weight</li> <li>• Add 1 foot long 3D-printed wing sections to both ends of the wing</li> </ul>

#### 2.4.2. CFD

The increased wingspan and extended fuselage of S.T.A.R. V2 results in a new aspect ratio of 8.028. Furthermore, the flat fuselage extension means a higher boundary layer growth, and thus an increased turbulence when separation occurs. Due to the relative flatness at both the fuselage extension and bottom of the airframe, the airframe may be approximated as a flat plate. Using a flat plate, the Blasius solution of the boundary layer can apply [16]. The Blasius solution at 99% of freestream velocity is used to roughly estimate the thickness of the boundary layer  $\delta$ , which is shown in Equation 4 [16].

$$\frac{\delta}{x} = 5.0 \text{Re}^{-\frac{1}{2}} \quad (4)$$

$$\text{Re} = \frac{\rho v L}{\mu} \quad (5)$$

In Equation 4,  $\delta$  is the boundary layer thickness,  $x$  is the length along the plate, and Re is the Reynolds number. The Reynolds number is calculated by Equation 5 to characterize the dominance of inertial or viscous forces in the flow where  $\rho$  is the density,  $v$  is the free stream velocity,  $L$  is the length of the flat plate, and  $\mu$  is the dynamic viscosity of air. Using the flat plate approximation, the maximum thickness of the boundary layer is approximated to be 4.163 mm when using the new length of S.T.A.R. V2 of  $L = 40$  in (1.017 m) and  $\mu$  as  $1.8 \cdot 10^{-5}$  Pa s [17]. To maintain the accuracy of the boundary layer and to provide a factor of safety against the extremely likely scenario that the boundary layer is much thicker than the results from the Blasius solution, a total of six 2 mm thick prism layer elements were chosen to surround the airframe. The prism layer is a specialized type of element specifically tailored to solve the

boundary layer effects. A quick calculation shows a factor of safety of 2.882 to account for the likely errors against the hand calculation approximations.

In addition, newer meshing schemes are explored in the second iteration of S.T.A.R. to improve technical accuracy and reduce computation time. STAR-CCM+ offers the choice between two types of meshing schemes: polyhedral (poly) and tetrahedral (tet) [11]. These methods discretize complex geometry into easy-to-solve geometric shapes. Both element types can be considered “good” using the cell quality statistic; a cell quality of 1.0 is considered a perfect element, which increases the likelihood of convergence, or in other words, an accurate solution [11]. A poly mesh typically yields a higher accuracy solution than a tet mesh, which leads back to the original decision of utilizing a poly mesh in the first analysis.

Observing Figure 23b, the poly mesh adheres poorly to geometry. The overall effect of higher accuracy in a poly solution may be lost due to the low quality of the polyhedral mesh, leading to higher errors in the solution. Thus, a tet mesh shown in Figure 23a is best suited for future analyses. Symmetry about the vertical and longitudinal axes plane is utilized to halve the computation time without compromising accuracy.

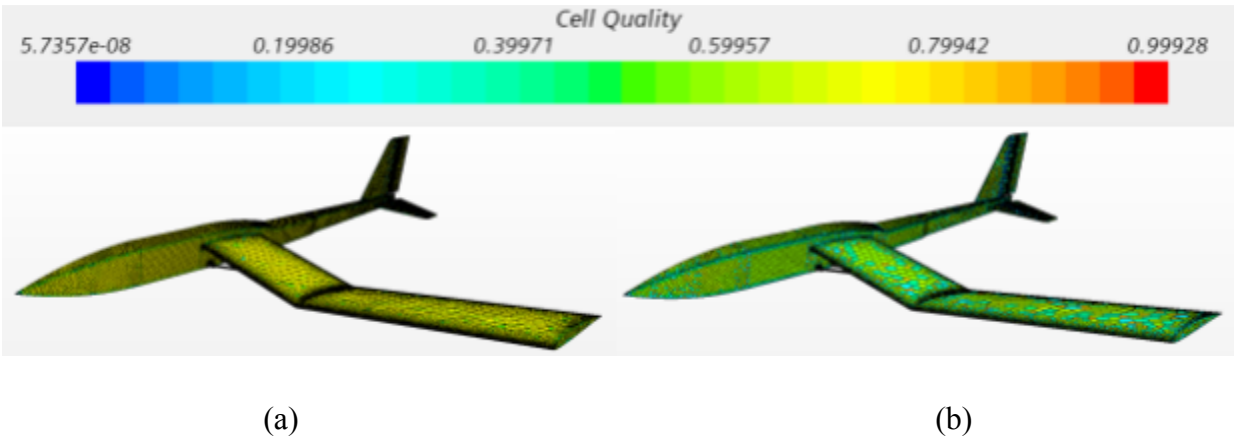


Figure 23: (a) Comparison Between Tet Mesh and (b) Poly Mesh

S.T.A.R. V2 is selected to be acceptable for iteration and a more comprehensive analysis is conducted. An experimental lift curve plot using data points for every  $2^\circ$  is calculated and displayed in Figure 24. Unsurprisingly, the lift curve looks similar to the airfoil curve in Figure 6 but shows lower values for  $C_l$ . While not perfect, estimations can be made that the zero lift angle of attack is maintained at around  $-2^\circ$  and the critical angle of attack is at  $12^\circ$ . As expected, the airframe will have worse performance than the infinite airfoil, leading to a maximum critical lift coefficient of 0.563 from the data before stalling.

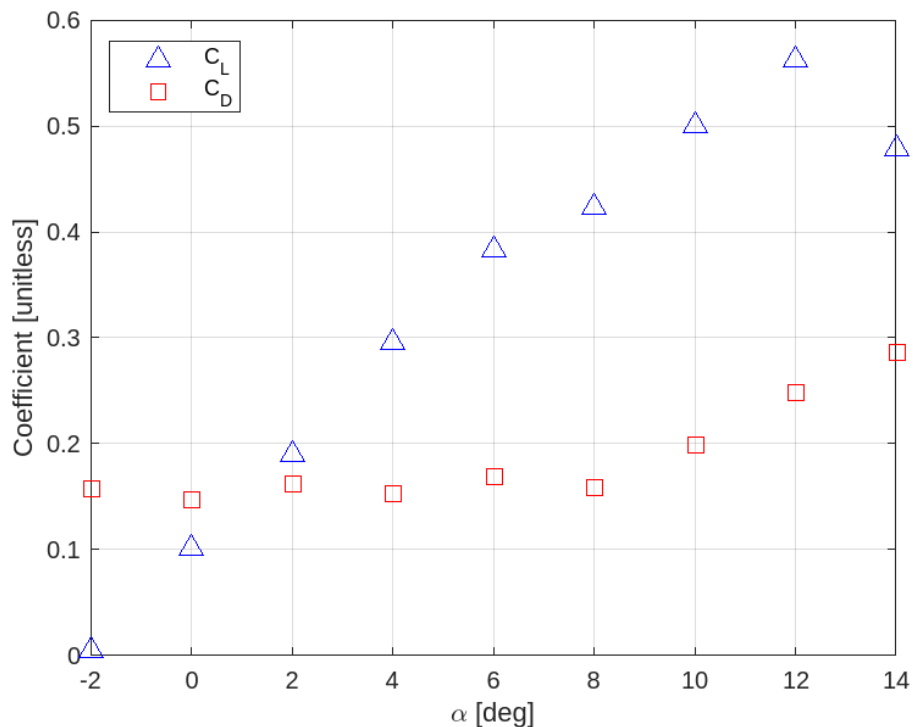


Figure 24: Coefficient Measurements

Furthermore, additional flight parameters are measured using the lift-drag ratio, which is shown in Figure 25. As stated previously in Section 1.2.3, the lift-drag ratio is characterized by dividing the lift by drag force, which works out to be equivalent to the glide ratio since the resultant force will be parallel to the direction of travel, assuming the glide conditions are not

changing. As presented in Figure 25, the maximum glide ratio  $E$  for S.T.A.R. V2 is 2.667, representing a 0.25 increase in a new glide ratio. Additionally, the best flight parameter for retaining lift is to pitch upwards within an  $\alpha$  between  $8^\circ$  to  $12^\circ$ . The V2 iteration's main drag component is dominantly in skin friction; only 5% is due to induced drag which presents a promising improvement.

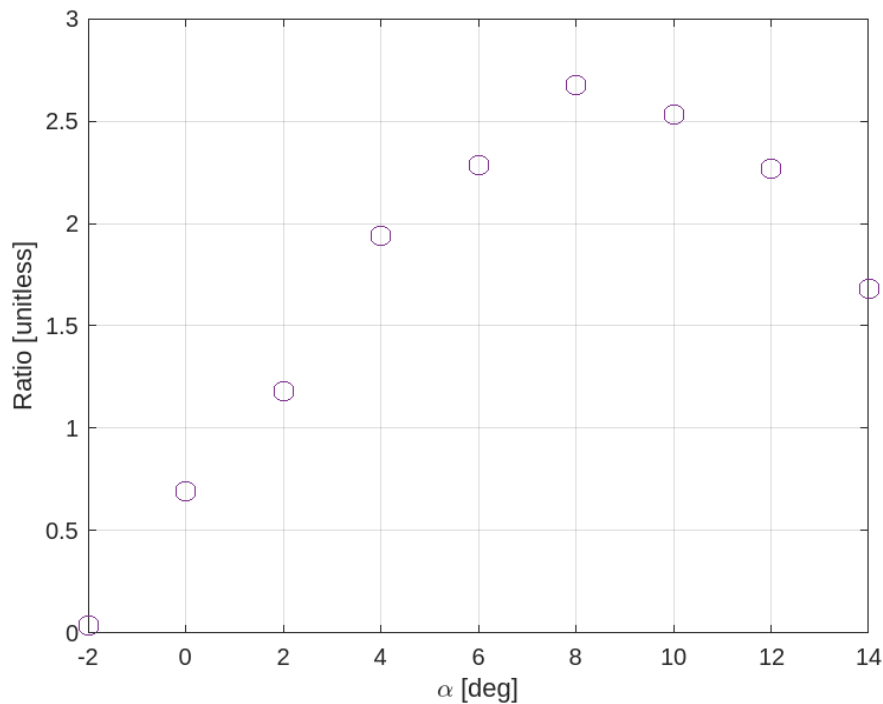


Figure 25: Glide Ratio Visualization

The critical lift coefficient represents the highest maximum aerodynamic forces that can act on the S.T.A.R.system. Figure 26 shows locations of high pressure where the supporting carbon fiber rods connect to the undersurface of the wing. These spots are caused by airflow encountering the support and curling upward due to zero velocity at the leading edges of the supports. The flow would then come in contact with the wings, which creates an additional stagnation point, leading to spots of higher pressure. Additionally, as the flow weaves through

the supports, there is a high potential for the boundary layer to detach, which typically results in vortex shedding in the flow.

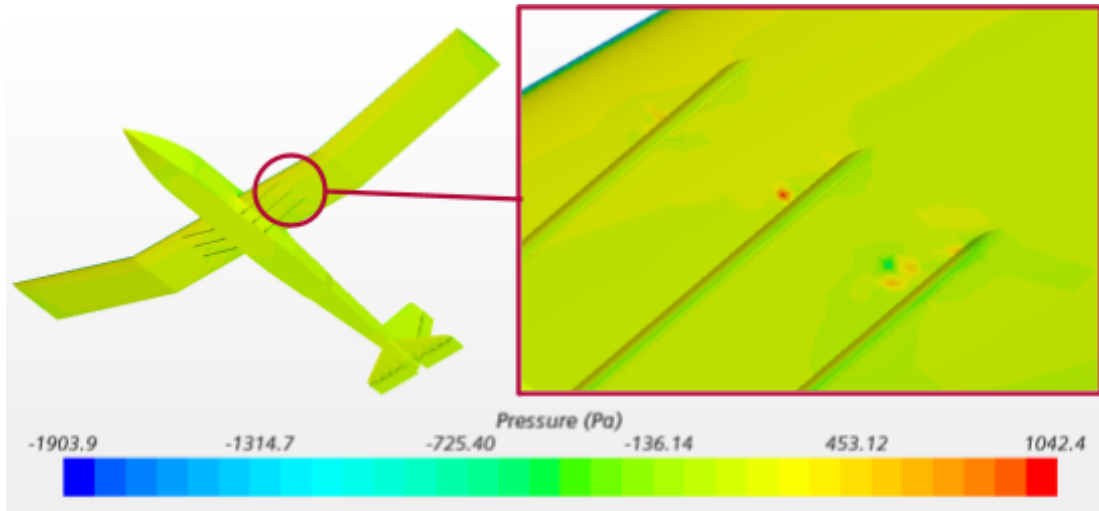


Figure 26: Wing Bottom Face Pressure Distribution

As the vortex sheds from the wing, this leads to a developing pressure gradient as the flow separates. The geometry of the body leads to the boundary layer detaching at different moments in time at the trailing edges. This oscillation leads to a cyclical load being imposed on the wing. If this vortex shedding frequency matches the natural frequency of the carbon fiber wings, this leads to flutter instability and eventual structural failure. The vortex shedding frequency can be characterized by the nondimensionalized Strouhal number, which is given in Equation 6 [18].

$$St = \frac{\omega L}{2\pi u} \quad (6)$$

Here,  $\omega$  is the vortex shedding frequency in radians per unit time,  $L$  is the length of the body, and  $u$  is the freestream velocity [18]. The Strouhal number depends on the Reynolds number; the

length can be estimated using both the chord of the wing and the length of the fuselage using the flat plate approximation purely as an estimate.

Using Equation 5, the Reynolds number can be calculated and a corresponding Strouhal number of approximately 0.22 can be found using Figure 27. Thus by rearranging Equation 6, one can find the vortex shedding frequency  $\omega$ . The length  $L$  can be calculated as the length of the chord of the wing, which is 0.150 m. Since both  $L$  and  $St$  are constant, that means that the frequency is expected to follow a linear relationship with the freestream velocity. This is demonstrated in Figure 28, which can also be used to reference the shedding frequencies in the testing velocity range.

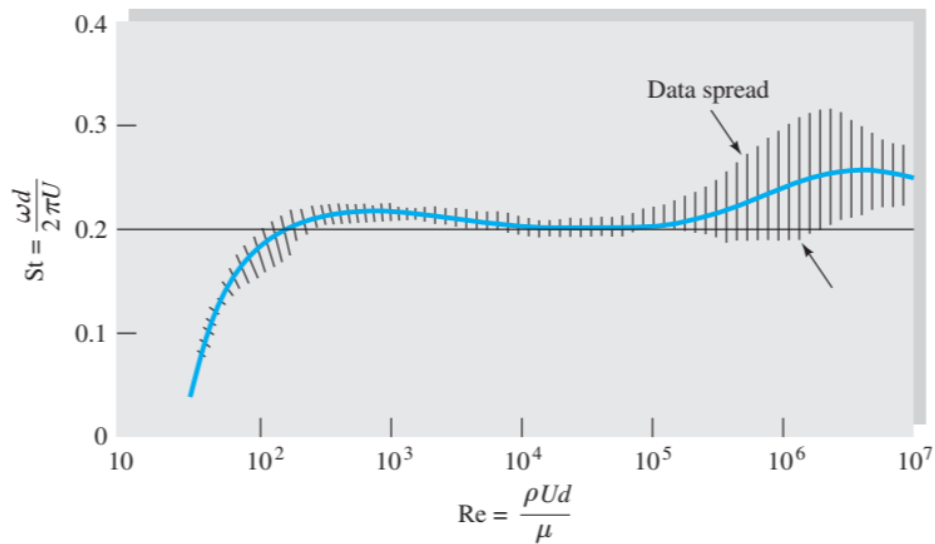


Figure 27: Experimental Shedding Frequencies [18]

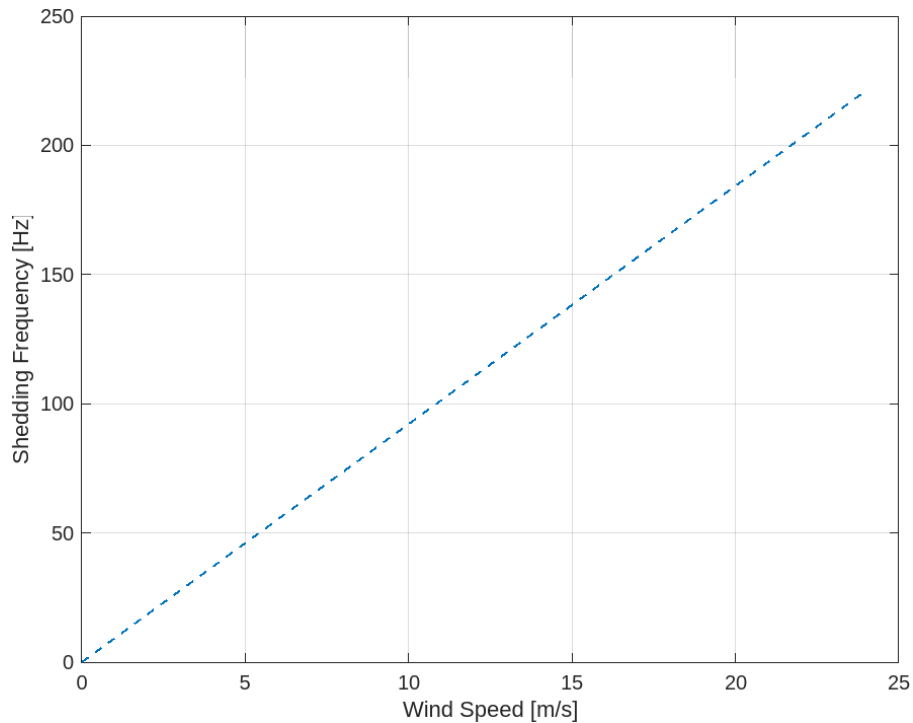


Figure 28: Visualization of Wing Shedding Frequencies

The wind speed is chosen slightly higher than the maximum testing speed of 22 m/s for additional safety. For reference, at the predicted maximum velocity of 22 m/s, the shedding frequency is found to be approximately 203 Hz. Further discussion is covered in Section 2.4.3 on the first five vibrational modes of S.T.A.R. V2's airframe. Regardless, S.T.A.R. V2 presents an improvement from V1 from a higher glide ratio and improved lift coefficient, and therefore a successful design iteration.

#### 2.4.3. FEA

More FEA simulations are run to determine structural integrity and the ability of S.T.A.R. to withstand pressure and force loading during flight. Assuming the identical conditions assumed for V1, an additional frequency simulation is run to ensure that vibrations won't cause failure.

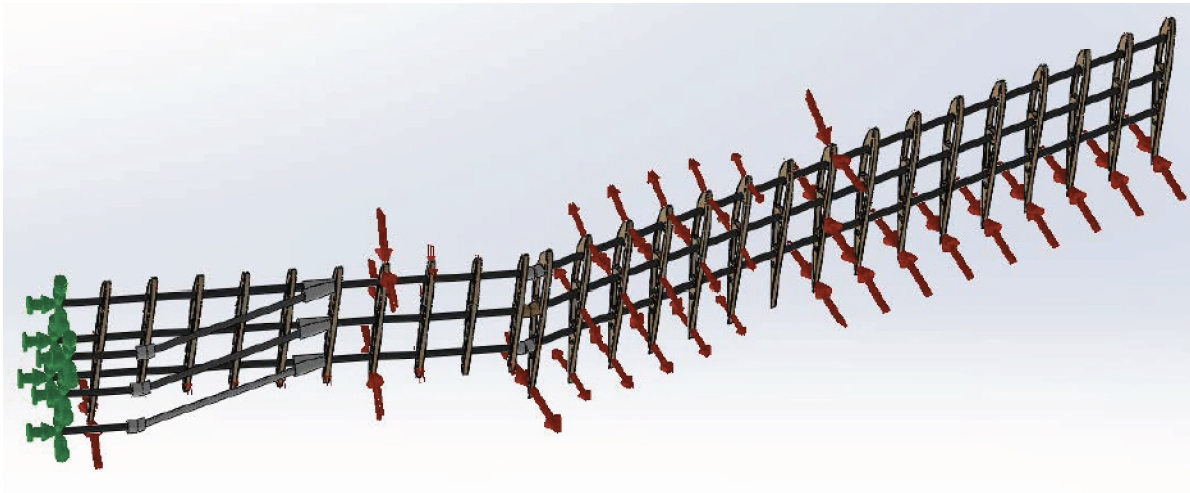
### 2.4.3.1 Stress Analysis

The focus of this FEA is to ensure the design will not fracture during flight by analyzing the material's ability to withstand stresses acting on the wings. Based on the numbers obtained from the CFD, the FEA can provide stress at each part of the wing. The Von Mises stresses will be able to show whether or not the individual pieces making up the wing will fracture or yield under high pressures. If the stresses exceed the yield strengths of the respective materials, the yielding materials need to be replaced with stronger alternatives. Table 5 lists the yield strengths of the materials used for the wing.

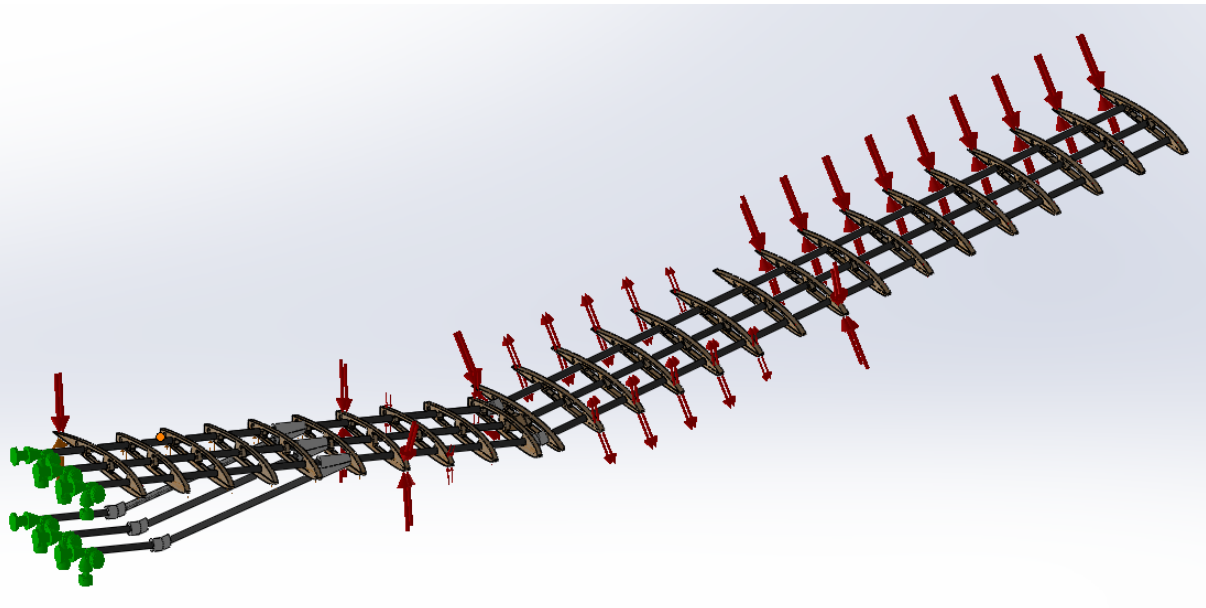
Table 5: Wing Yield Material Properties

<b>Material</b>	<b>Yield Strength (MPa)</b>
Basswood	40.7
Carbon Fiber	5000
PLA	60

Because the output stresses are important for this study, the setup has to be accurate and detailed. The pressure distributions are taken from the CFD, but the gradients are not assumed to be uniform across the span of the wing anymore. The pressure values are estimated for each section of the wing using the probe in STAR-CCM+. Those point values are then curve-fit with Excel so that the equations can be input into SolidWorks. With the addition of small PLA parts and a more complex pressure distribution, the computation time increases. To keep the computation time low, only half of the wing will be simulated with the assumption that the other side is identical due to symmetry. The final setup is pictured below in Figure 29.



(a)

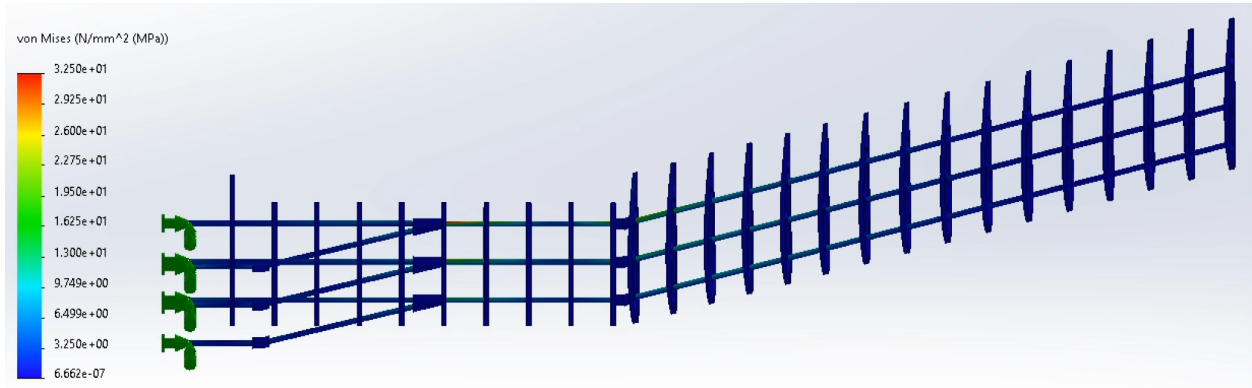


(b)

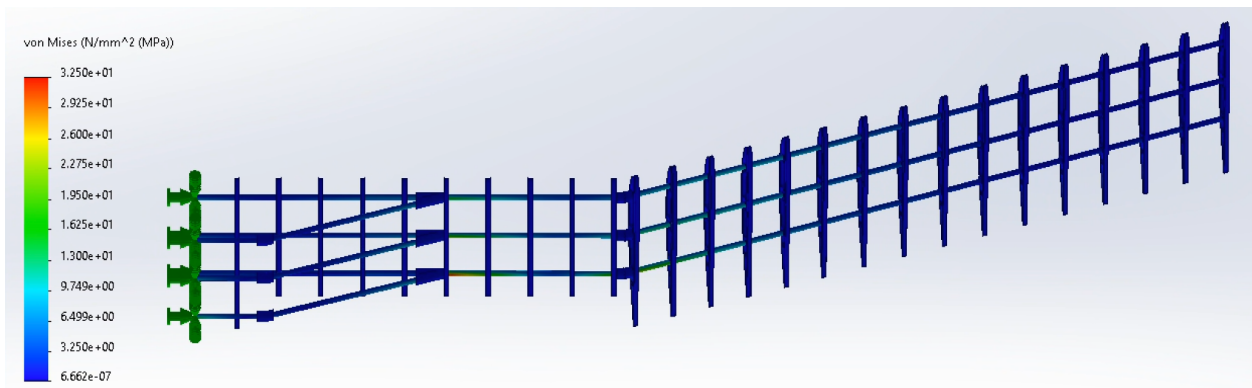
Figure 29: (a) Pressure Distributions on the Bottom and (b) Top of the Wings

After running the simulations, the von Mises stress plot is displayed with a color bar to demonstrate the stress change across the wing as seen in Figure 30. Figure 31 zooms in on a critical part right where the wing meets the lower support bars. This is consistent with the CFD results where the highest pressure existed near the connection point just above the support bars.

Although this is a point of high stress, the stress reading of 32.5 MPa is magnitudes less than carbon fiber's yield strength, 5000 MPa. In the same manner, the stress on the wood spars reads only about 3.25 MPa which is also nowhere near the yield strength of basswood, 40.7 MPa.



(a)



(b)

Figure 30: (a) Von Mises Contours Along the Top and (b) Bottom of the Wing

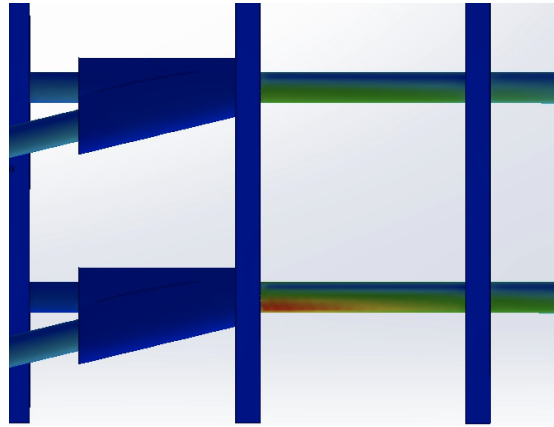


Figure 31: Critical Stress Location

#### 2.4.3.2 Frequency Analysis

For further reference, the first five vibrational modes are tabulated in Table 6. According to Figure 28, there will be one specific freestream velocity at which the shedding frequency matches that of the first mode occurring at 25.96 Hz, as seen in Figure 32. This occurs at about 2.8 m/s, but would only be at precisely that speed. An interesting note is that the entire range of testing velocities lead to shedding frequencies equivalent to the first five modes.

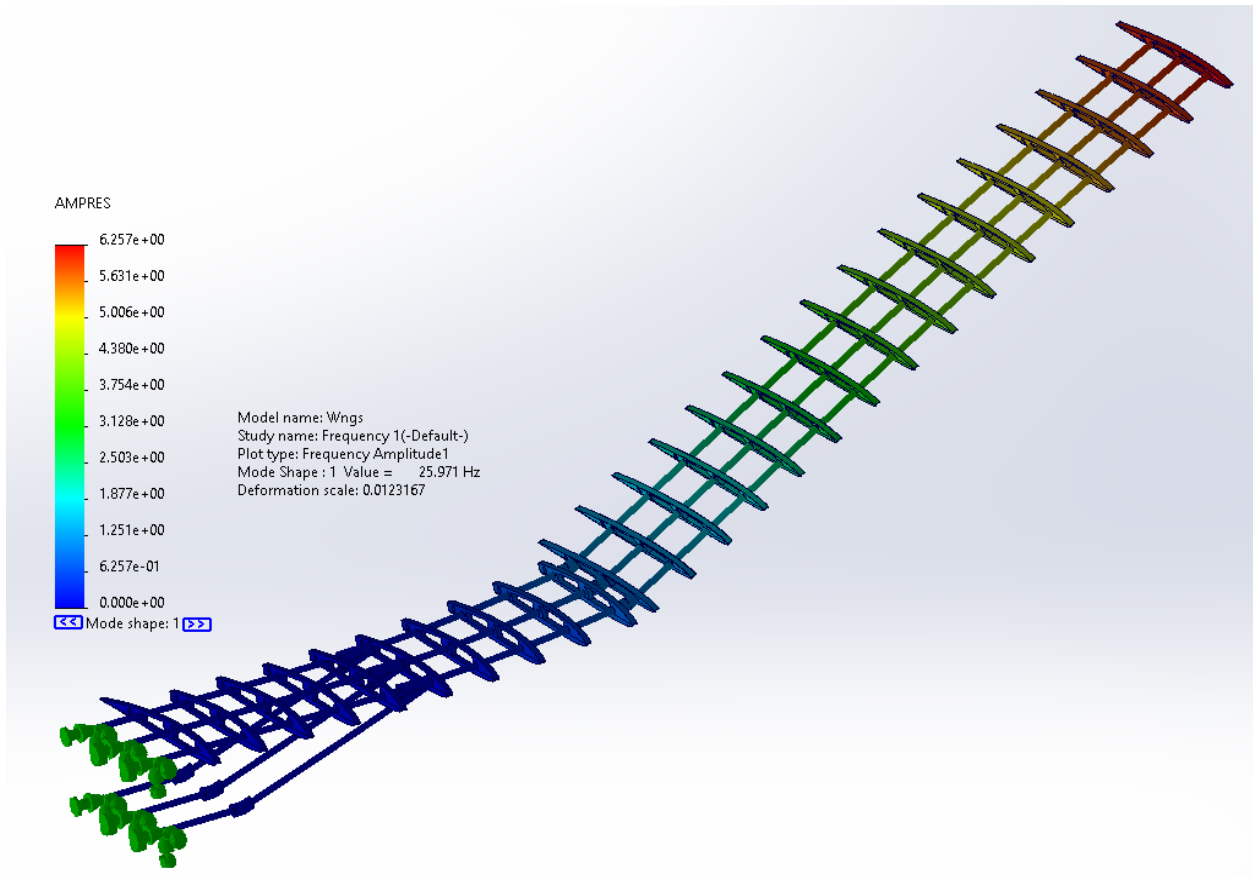


Figure 32: Resultant Vibrational Amplitudes at the Wing Natural Frequency

Table 6: Modal Frequencies

Mode Harmonic [unitless]	Frequency [Hz]
0	25.96
1	49.303
2	94.723
3	136.63
4	210.42

Due to variations that take place during flight, it can be reasoned that it is incredibly unlikely that S.T.A.R. V2 will consistently maintain constant velocity. Such a small time window to maintain resonance means that the wings will more likely follow beating. It can be concluded that flight at

a transient velocity time frame will not lead to structural failure. In summary, the FEA confirms that the wing can withstand the pressures exerted on it during flight.

#### 2.4.4. Manufacturing Decisions

In order to address the unideal center of gravity of the glider, weight is reduced on non-load-bearing components such as vertical stabilizers, rudders, ailerons, and several parts of the fuselage. Holes are drilled and larger pieces are cut out of the wood before covering them with solar film. This film is heated using a hot iron and heat gun in order to shrink and adhere the material to the surfaces. The overall mass of the glider is decreased and significant weight removal from behind the wings causes the center of gravity to move closer to the desired position of a quarter chord length behind the leading edge of the wing. This also means that less ballast would need to be added to the nose of the glider in order to move the center of gravity to the quarter chord.

The wingspan extension of Version 2 is accomplished through 3D printing. This reduces build time and ensures straight and uniform wings. 3D printing effectively remedies both issues found when manufacturing the wing from basswood cross sections with carbon fiber wing spars. One disadvantage of 3D printing the wings comes in the form of weight. Each 6-inch long wing section is 5 grams heavier than an equivalent 6-inch section of wing built from the wood cross sections.

#### 2.4.5. Wing 3D Printing

In order to minimize the weight of the printed wing sections, the CAD models are optimized for vase mode printing (called Spiralize Outer Contour in Ultimaker Cura slicer). Each 12-inch long wing extension is split into two six-inch pieces since that is the maximum the z-axis

can accommodate. Vase mode only prints the exterior wall of a solid body, and will not print any interior volume of the part. In order to incorporate strengthening ribs for single outer continuous line printing, an array of rectangles with a common wall thickness of 0.1mm is extruded and made into a separate body from the wing, henceforth referred to as the grid body. A 0.6 mm thick groove coincident with the camber of the wing is removed from the grid body. After these operations, the original wing should be left untouched and the grid body should be separated with the 0.6mm groove in the middle as shown in Figure 33. Additional weight-reduction holes can be made in the grid body. Any material removed from the grid body will be material not present on the internal ribs of the wing. Holes for attaching the carbon fiber rod wing spars are added by removing a cylinder directly from the original wing body. Finally, the modified grid body is subtracted from the original wing, allowing the original to be printed in vase mode including the internal ribs, resulting in a wing resembling Figure 34. Because the walls of the grid body are so thin (0.1mm), the adjacent walls will be printed as a reinforcing rib that extends through the wing interior. The groove thickness of 0.6mm is chosen because it is a distance large enough for the slicer software to recognize the walls as distinct features, but close enough that the tolerances of the printer will cause the gap to close, making a stronger rib. The view of the vase mode with internal ribs is shown in Figure 35. In order to check that the internal structure will be correctly sliced by the software, the viewing mode is changed to the translucent “X-Ray” mode, similar to Figure 36, so that the internal cuts and weight reliefs become visible. Figure 37 shows the printed result of the sliced file shown in Figure 35.

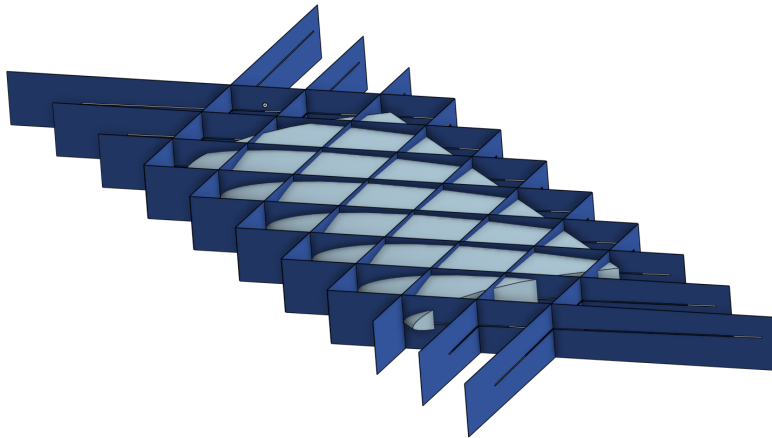


Figure 33: Wing (light blue) with Grid Body (dark blue) with center slot removed.

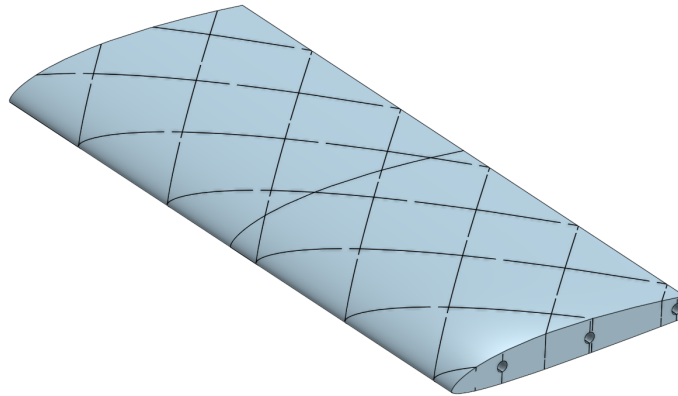


Figure 34: CAD Result of Wing with Vase Mode Optimizations and Internal Ribs

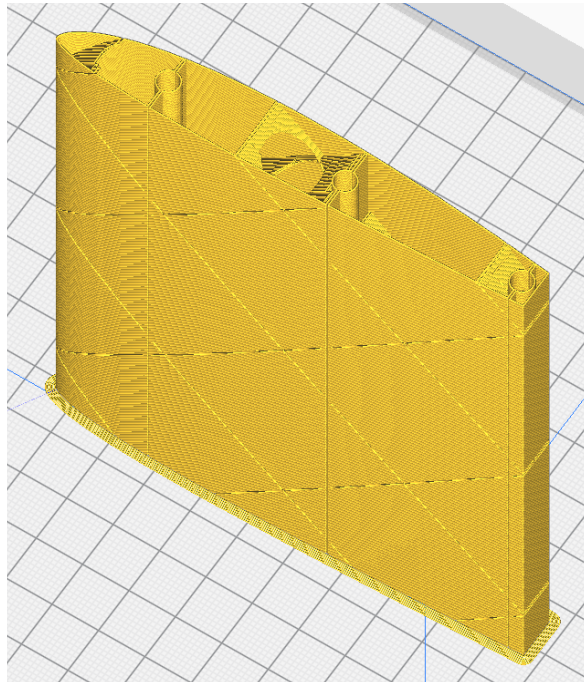


Figure 35: Ultimaker Cura Slicer View of Vase Mode Wing

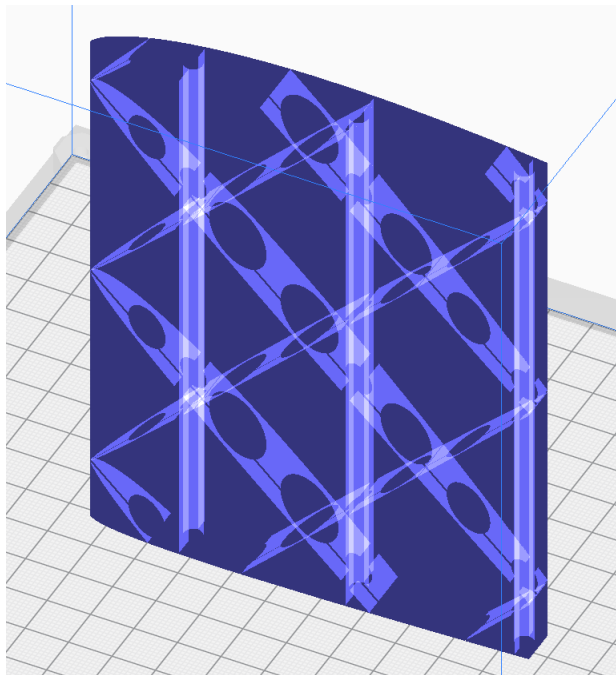


Figure 36: X-Ray View of Cura Vase Mode Wing Slicing

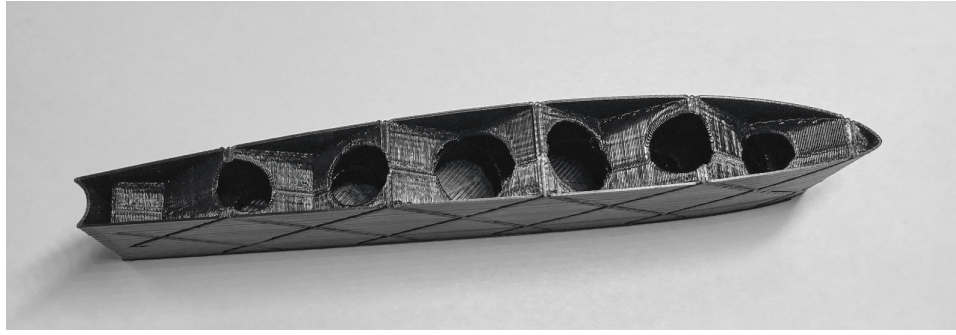


Figure 37: Final 3D-Printed Wing Cross Section

#### 2.4.6. Construction

Once all four wing additions are printed from PLA+ material, they are attached to the existing wing by inserting the existing carbon fiber rods into the holes designed to connect the additions together. Super glue is then used to assemble the wing sections together. Around the tips of the existing wing, the solar film is removed in order to allow the super glue to stick to the basswood beneath. The film is then replaced with a single piece wrapped around each junction. The 3D-printed parts are left uncoated since their surface finish is already relatively smooth.

### 3. Testing

With the version 2 design complete, the S.T.A.R. system needs to be evaluated according to the design requirements. In order to simulate the conditions under which the system would enter the glide phase, it is dropped from a tethered weather balloon and then piloted back to the launch location.

#### 3.1. Testing Location

Verification of the S.T.A.R. system requires a live drop test from the weather balloon to simulate the actual environment. All testing takes place at the Santa Clara County Model Aircraft Skypark (SCCMAS). Table 7 lists the following dimensions of the airfield at SCCMAS.

Table 7: Airfield Dimensions [19]

Location	Length [ft]	Width [ft]	Height [ft]
Main Runway	516	60	500
Taxi Line	100	100	500
Pit Area	100	100	500
Total Area	1,122	160	500

To obtain permission to use the field at SCCMAS, the team reaches out to Mike Legget, a Secretary on the Board of the SCCMAS. Due to Legget's experience in RC plane flight, the team nominated Legget to be the pilot for the drop tests.

#### 3.2. Initial Glide Test & Control Surface Trimming

In order to gauge the current trim settings on the Flysky FS-i6 6CH 2.4GHz AFHDS RC Transmitter, an initial running glide test is performed. This is accomplished by running with the

glider parallel to the ground until the glider naturally lifts from the hands of the testing participant. From there, the glider is allowed to freely fly before Legget attempts to pitch the glider up toward the end of its descent. Observations made by Legget and the team leads to necessary troubleshooting resulting in trimming the vertical and horizontal stabilizers in order to prevent unwanted pitch and yaw imbalance as shown in Figure 38. This involves utilizing the programmed controller to adjust the control surfaces to an aerodynamically balanced position. Additionally, Legget noted that the sensitivity of the controller was too high. This meant that the deflection range of each control surface exceeded the ideal amount. This could cause the glider to overreact and potentially lose control in flight. To address this, Legget worked with the team to adjust the sensitivity of each control surface, dropping the sensitivity of all channels from 100% to 50% in both the positive and negative directions.



Figure 38: Control Surface Sensitivity Adjustment

### 3.3. Experimental Setup

Pre-test evaluations of the S.T.A.R. system are completed in order to ensure responsive controls. The weather balloon is then filled with sufficient helium to provide positive lift to the entire system. Upon reaching the maximum tethered altitude, S.T.A.R is released and enters the glide phase.

#### 3.3.1. Helium

With a payload weight of 998 g, sufficient helium is needed to fill the 600 g weather balloon to ensure a timely and sustained ascent. Average values from traditional weather balloon systems are used in order to most accurately represent test conditions. For calculations, the glider and payload mass is rounded to 1 kg to both simplify and slightly overestimate values to ensure proper ascent.

To calculate the necessary amount of helium, the total system weight and desired positive lift are taken into account. With an average positive lift of 250 g, balloon mass of 600 g, and payload weight of 1 kg, the total effective lift needed from the helium is 1,850 g (Table 8). Conservatively, one cubic foot of helium has a lift of approximately 27.82 g [20]. This estimation is used to ensure that calculated helium meets or slightly exceeds the necessary amount. Dividing the total system mass by this lift approximation (per cubic foot) yields a required 66.49 cubic feet of helium needed to satisfy the set requirements. For S.T.A.R. system testing, tanks of helium are acquired from Party City with each containing enough gas to occupy 14.9 cubic feet for room temperature conditions at 1 atmosphere (80% helium to 20% air mixture by volume). Assuming each cubic foot of this mixture possesses 80% of the lift of pure helium, a minimum of (5.57) 6 tanks have to be purchased. Although air's unideal density contribution will cause a

lower final altitude and slowed ascent, this mixture is acceptable at low testing altitudes (250 feet). In comparison, professionally launched weather balloons utilize pure helium to maximize lift per cubic foot which allows for smaller and lighter balloons. Due to the unreliability of nonindustrial helium tanks, 8 tanks are purchased to ensure sufficient lift. High Altitude Science’s proprietary balloon calculator predicts an ascent rate of 2.94 meters per second which is more than sufficient for testing purposes [21]. Based on this same calculator, the release of the balloon with no tether results in a rise to 29,230 meters or 95,899 feet. This altitude is comparable to altitudes that traditional weather balloon systems reach.

Table 8: Parameters for Helium Calculation

<b>Known Parameter</b>	<b>Value [various]</b>
Payload Mass	1 kg
Weather Balloon Mass	600 g
Required Balloon Positive Lift	250 g

### 3.3.2. Connections

Several connections are fabricated in order to carry out the testing procedure. A vinyl tube is cut to approximately 5 feet and is responsible for connecting the helium tank to the balloon inflator adapter (Figures 39 and 40). This adapter is then placed into the neck of the weather balloon to allow inflation. The balloon inflator adapter is modeled in OnShape software and is manufactured using the same FDM 3D printers used to manufacture the wing extensions.

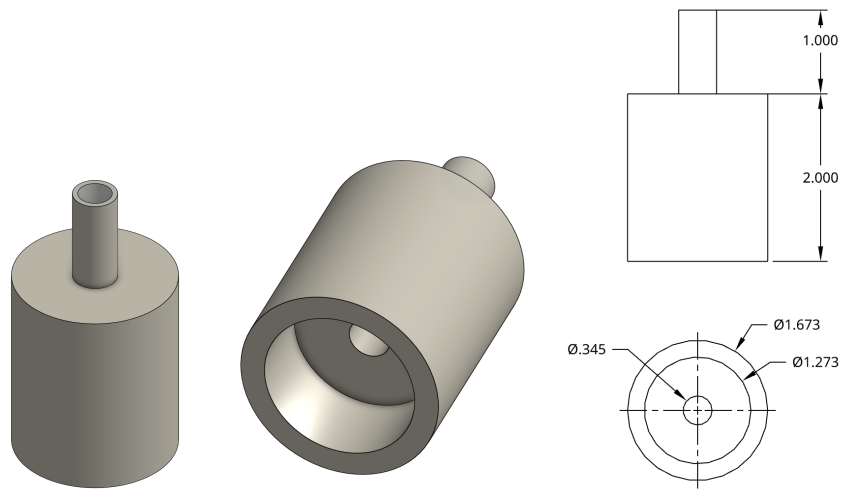


Figure 39: Weather Balloon Inflator Adapter



Figure 40: Inflated Balloon and Hose Connection

The connector from the vinyl tube to the helium tank is created by utilizing two small party balloons. Two party balloon necks are cut off, ensuring one is slightly longer than the other. The shorter neck is concentrically stretched and then placed onto the longer neck. The two balloon necks are then placed onto one end of the vinyl tube and a rubber band is attached to create an airtight connection between the tube, party balloon necks, and helium tank.

Once the balloon is fully inflated and ready to be released, electrical tape, rubber bands, and fishing wire are attached to the balloon in order to anchor it down as seen in Figure 40. A 10-pound fishing line is used as a tether to ensure an altitude of 200 feet was maintained. The fishing line is laid out on the runway in 250-foot lengths and doubled back six times in order to make a stronger bundle of lines. This results in six identical lines that give an approximate tensile strength of 60 pounds for the balloon tether. The line is then wrapped several times around the weather balloon's neck before several loops of electrical tape are applied. After the first application, the fishing wire is alternately wrapped in electrical tape. One wrap is done by holding the fishing wire in the upwards direction, followed by a wrap while holding the wire in the downward direction. This is repeated until the connection is secure. The other end of the fishing line is tethered to a chair that one of the team members was sitting in to secure the connection. This connection is monitored throughout the tests.

### 3.3.3. General System and Release Mechanism Test

Once the fishing line is attached to the balloon, the release mechanism and general system are both tested before launch. For the general system testing, all control surfaces are observed as the controller attempts to actuate each servo motor throughout their full range of motion. Once this was seen as successful, the release mechanism is tested by turning the respective knob on the controller and observing whether or not the glider falls downwards into

one of the participant's hands as shown in Figure 41. Throughout the first two attempts, the release mechanism did not seem to receive any signal from the controller. After resetting the power on the glider, the release mechanism became responsive and successfully released the glider. This is retested twice before the glider is cleared for launch.



Figure 41: Balloon Release Mechanism Test

### 3.4. Test 1

Once the glider reaches approximately 200 feet, the release mechanism is activated as shown in Figure 42. The glider falls nose down for 20 feet before the pilot pulls out of the dive and enters the glide phase. The first 100 feet of S.T.A.R.'s descent is smooth with little to no turbulence. During this period, S.T.A.R. maintains an impressive altitude and its flight plane is parallel to the viewing plane of the launch point. In the first section of the glide, S.T.A.R. is piloted in the same direction of the wind which allows for the initial smooth flight.



Figure 42: Initial Release

In the last 100 feet, the pilot attempts to change course in order to bring the glider back toward the launch location for landing. This requires the pilot to make a sharp turn perpendicular to the wind. S.T.A.R. faces several bouts of turbulence, speed decrease, and unwanted roll. This turbulence is short-lived and S.T.A.R. eventually stabilizes and is able to successfully make the necessary trajectory adjustment as seen in Figure 43. Once close enough to the ground, the pilot pitches upwards and the glider successfully skid-lands in the designated return area located on the edge of the runway (Figure 44). Traveling a total of 40 seconds and approximately 600 horizontal feet, a 3:1 glide ratio is achieved for Test 1.



Figure 43: Final 100 Feet of Test 1



Figure 44: Moments Before Skid Landing on Runway

Upon landing, some of the weights that were placed in the nose of the glider (in order to move the center of gravity forward) broke out of the fuselage. The battery pack located within the nose also becomes loose and needs readjustment before the next flight. Upon retesting the control surfaces and release mechanism, some inconsistencies occur. For example, the control surface response is no longer reliable and connectivity cuts in and out. This is most likely due to unsoldered wire connections near the receiver coming loose upon landing. Even knowing that the system is facing connectivity issues, another test is still conducted to gather as much information regarding release mechanism reliability and performance under unideal system conditions. A completely unresponsive system would also give valuable insight into S.T.A.R's structural integrity after a hard impact.

### 3.5. Test 2

To commence the second test, the weather balloon is pulled down by hand until it arrives at its initial launch point. The release mechanism is reattached to the glider and connections are double-checked before the second launch commenced. The release tests yield connection uncertainty but the launch was nevertheless continued. The balloon is released to a similar altitude of approximately 250 feet and the group gives an all-clear to the pilot for system release. The glider successfully releases from the balloon but as expected, the control surfaces receive no signal from the controller. The actuation of the release mechanism followed by unresponsive control surfaces give further reason to believe that the un-soldered connections were at fault rather than the controller itself. Upon deeper investigation, the servo gear teeth were actually sheared off inside the gearbox, leading to no contact and therefore loss of control. This may have been due to the heavy impact of the skid landing in Test 1. The complete lack of control surface

actuation causes the glider to move at the mercy of the wind before the crash landing in the fields, shown in Figure 45. Even after a complete fall from 250 feet, most of the S.T.A.R. is intact except the nose of the fuselage which takes most of the force. The structural impulse load capabilities of the S.T.A.R. system are proven to be relatively impressive and are attributed to the use of basswood instead of more traditional small aircraft wood such as balsa.



Figure 45: S.T.A.R. in the Field

## 4. Conclusion & Next Steps

S.T.A.R. system tests are evaluated against design requirements and further analyzed, highlighting beneficial design changes for future iterations of the glider.

### 4.1. Satisfaction of Design Requirements

Evaluation of S.T.A.R. testing demonstrates sufficient flight control and housing for weather-sensing equipment. The design requirements and observed results are summarized in Table 9.

Table 9: Test Results

<b>Design Requirement</b>	<b>Test Performance</b>
Full yaw, roll, and pitch adjustment to direct glider towards desired landing position	Complete flight control during test
Glide ratio > 1:1	Actual glide ratio $\geq$ 3:1
GPS location transmission	Not tested
Houses GPS, humidity, pressure, and temperature sensors	Achieved
Sensor data collection	Achieved
Total weight of 1 kg or less	Final Total Weight: 998 g
Reusable & Weather Resistant	Successful landing, partially reusable. Solar Film resists water

### Flight Control

During Test 1, Legget demonstrates complete yaw, roll, and pitch control, and successfully navigates the glider back to the launch location.

### Glide Ratio

An approximate glide ratio of 3:1 exceeds the initial design requirement by a factor of 3 and displays the successful aerodynamics of the S.T.A.R. system.

### Equipment Housing & System Weight

The S.T.A.R. system successfully housed GPS, humidity, pressure, and temperature sensors within the fuselage. The maximum system weight requirement of 1kg is cleared by 2 grams with a final total system weight of 998 grams.

### Sensor Data Collection & GPS Location Transmission

Weather data is successfully collected while in the S.T.A.R. system. GPS location transmission is not tested due to electronic malfunction but is included onboard to mimic proper flight conditions.

### Reusable

Although the ultimate goal of the S.T.A.R. system is reusability, future iterations need to have greater structural resilience. Complications involving loose wiring after Test 1 will be addressed by moving all wiring to a dedicated PCB board and ensuring complete soldering of the electrical system. Onboard battery packs additionally need housing to ensure increased stability upon landing. After testing, parts of the 3D-printed PLA wing not wrapped in the solar film began deforming after being exposed to continuous sun for ~20+ minutes.

## 4.2. Future Prototype Iterations

A fully integrated control system and manufacturing methods need to be evaluated in order to increase the future functionality of the S.T.A.R. system.

### 4.2.1. Manufacturing Decisions

Future S.T.A.R. prototypes will be manufactured using primarily 3D-printed parts, foam, and carbon fiber rods. A tentative design of S.T.A.R. Version 3 is shown in Figure 46.

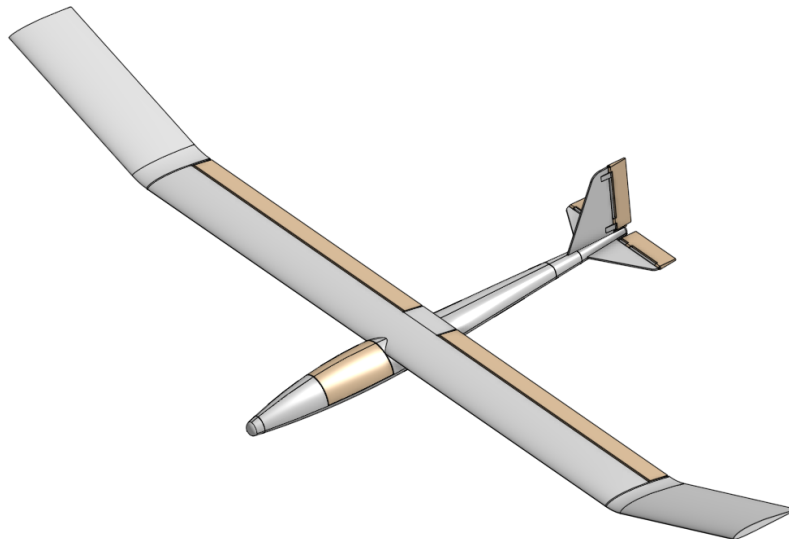


Figure 46: Proposed CAD for Version 3

Switching from a basswood majority construction to 3D-printed plastic will decrease the construction time in addition to allowing for more flexibility and reproducibility during the design process. One major improvement for future iterations is the change from PLA+ filament to a UV-resistant polymer with a higher glass transition temperature. These new polymer properties help prevent 3D-printed parts from deforming in intense heat or UV exposure. One such filament (ASA) can be printed on desktop FDM printers but requires a heated bed and strict ambient temperature control. These considerations necessitate an enclosure around the printer

that contains the generated heat. Another 3D printing improvement involves using smaller nozzles such as 0.3mm or even 0.2mm. These smaller nozzle sizes can increase part strength, surface finish, and print resolution. For the 3D-printed wings of the S.T.A.R. system, the team observes that the internal ribs of version 2 were sufficiently and exceedingly strong. This allows the minimum wall thickness to be reduced from 0.4mm to smaller sizes. Although this is still possible with a 0.4 mm nozzle, creating walls thinner than the nozzle diameter can lead to imperfections and reduce part strength. It is for this reason that smaller nozzle sizes would be ideal for the manufacturing of the S.T.A.R. system.

Transitioning S.T.A.R. system manufacturing from laser-cut wood to FDM-printed parts allows for more complex geometry and higher precision assembly. This allows for a cylindrical fuselage, shown in Figure 46, rather than the rectangular geometry previously manufactured using the laser cutter, seen in Figure 21. The cylindrical fuselage additionally helps reduce the cross-sectional area and drag coefficient. While laser cutting is more efficient than plastic extrusion, the glue-up time and tolerance stack-ups for wood negate any speed benefits of laser cutting. For manufacturing of the S.T.A.R. system, assembly time, weight, and part consistency must all be considered together, rather than on an independent basis.

#### 4.2.2. Future Construction Practices

The 3D-printed wings will be assembled by feeding carbon fiber rod spars into designated holes in the wing. To assist in connection, super glue will be used for general adhesion. For sections of the fuselage that have very thin walls, flanges will be included in the CAD model to create lap joints for more gluing surface area. Although future iterations will mainly include 3D-printed parts, replacing wood glue from the assembly and replacing it with instantly bonding anaerobic adhesive would drastically decrease assembly time. This would also

function as a tolerance check for bonded components and reduce the number of consumables on the Bill of Materials.

### 4.3. Projected Large-Scale Implementation and Mass-Production

The design and manufacturing process in the first two versions of the S.T.A.R. system prove its potential for large-scale implementation. Future iterations require a refined manufacturing process that minimizes material costs and streamlines production.

#### 4.3.1. Design Changes

Future iteration of the S.T.A.R. system must ensure weather sensors are exposed to the atmosphere for proper data collection. This requires designing interior housings at locations that expose sensors while maintaining a consistent fuselage shape. This design change poses less of a complication with updated production methods.

Once the prototypes are able to consistently demonstrate fully autonomous navigation to a predesignated landing location, the production methods can be altered for large-scale implementation and mass production. Such changes include molds for foam fuselages and injection molds for wing sections that could be designed for poka yoke, ensuring perfect assembly through initial error reduction. Using molds to manufacture the fuselage and wing components and building dedicated PCBs would be the best way to reduce the cost and complexity of the S.T.A.R. system. The tests demonstrated that data could be collected within the fuselage, but it is likely that the PCBs or some of the sensor probes will need to be mounted on the exterior of the plane to get much more accurate readings. Especially at higher altitudes where the sensor values will be significantly different from those obtained during the low-height tests.

Cost and complexity reduction would ultimately lead to an increased eagerness from companies to invest and learn about the benefits of the S.T.A.R. system.

#### 4.3.2. Expected Cost of Production

High-volume production initially entails large tooling setup costs which are consistent with other manufacturing methods. Because the raw glider materials are inexpensive and the electronic components can be off the shelf, a reasonable assumption for the total cost of the body, wings, electronics, and motors would be \$100. Over time, these costs would decrease due to high volume discounts from manufacturers. Additionally, if parts are molded from foam and thermoplastics, combined manufacturing costs could drop as low as a few dollars in raw materials. However, the initial mold investment cost would only be offset at very high production volumes and could not feasibly be integrated too early into the product launch.

## 5. References

- [1] One Degree of Freedom Approach for an Autonomous Descent Vehicle Using a Variable Drag Parachute - Scientific Figure on ResearchGate. Available from:  
[https://www.researchgate.net/figure/High-altitude-balloon-payload-system-configuration-When-balloon-bursts-or-is-released\\_fig7\\_268581379](https://www.researchgate.net/figure/High-altitude-balloon-payload-system-configuration-When-balloon-bursts-or-is-released_fig7_268581379) [accessed 13 Jun, 2023]
- [2] NOAA. “Weather Balloons.” *National Weather Service*, 8 Oct. 2020,  
[www.weather.gov/bmx/kidscorner\\_weatherballoons#:~:text=Weather%20balloons%20are%20the%20primary,storms%2C%20and%20data%20for%20research](http://www.weather.gov/bmx/kidscorner_weatherballoons#:~:text=Weather%20balloons%20are%20the%20primary,storms%2C%20and%20data%20for%20research).
- [3] “U.S. Standard Atmosphere vs. Altitude.” *Engineering ToolBox*, 2003,  
[www.engineeringtoolbox.com/standard-atmosphere-d\\_604.html](http://www.engineeringtoolbox.com/standard-atmosphere-d_604.html).
- [4] Krueger, Jason. “How Much Weight Can a High Altitude Weather Balloon Carry?”  
*StratoStar*, 7 Feb. 2023,  
[stratostar.com/how-much-weight-can-a-high-altitude-weather-balloon-carry/#:~:text=Cell%20phones%20are%20not%20permitted,balloon%2C%20cannot%20exceed%2012%20pounds](http://stratostar.com/how-much-weight-can-a-high-altitude-weather-balloon-carry/#:~:text=Cell%20phones%20are%20not%20permitted,balloon%2C%20cannot%20exceed%2012%20pounds).
- [5] “Environmental Impact of Radiosondes.” *Environmental Impact of Radiosondes | NORIS Group GmbH*, 16 July 2020,  
[www.graw.de/company/philosophy/environmental-impact-of-radiosondes/#:~:text=The%20nylon%20cord%20commonly%20used,offer%20an%20alternative%20cotton%20cord](http://www.graw.de/company/philosophy/environmental-impact-of-radiosondes/#:~:text=The%20nylon%20cord%20commonly%20used,offer%20an%20alternative%20cotton%20cord).
- [6] “Styrofoam #6 Expanded Poly-Styrene (EPS): Athens-Clarke County, GA - Official Website.” *Styrofoam #6 Expanded Poly-Styrene (EPS) | Athens-Clarke County, GA - Official Website*,

[www.accgov.com/8224/Styrofoam#:~:text=Styrofoam%20\(more%20appropriately%20called%20Polystyrene,possibly%20much%20longer%20-%20to%20decompose](http://www.accgov.com/8224/Styrofoam#:~:text=Styrofoam%20(more%20appropriately%20called%20Polystyrene,possibly%20much%20longer%20-%20to%20decompose). Accessed 1 June 2023.

[7] Anderson, J., 2017, **Fundamentals of Aerodynamics Sixth Edition**, McGraw-Hill, New York. pp 326.

[8] *New Airfoils for R/C Sailplanes*, 21 Mar.1997,  
[m-selig.ae.illinois.edu/uiuc\\_lsat/saAirfoils.html](http://m-selig.ae.illinois.edu/uiuc_lsat/saAirfoils.html).

[9] Anderson, J., 2017, **Fundamentals of Aerodynamics Sixth Edition**, McGraw-Hill, New York. pp 1095.

[10] “Choosing the Right Turbulence Model for Your CFD Simulation.” *Engineering.Com*,  
[www.engineering.com/story/choosing-the-right-turbulence-model-for-your-cfd-simulation](http://www.engineering.com/story/choosing-the-right-turbulence-model-for-your-cfd-simulation).  
Accessed 22 Aug. 2023.

[11] Siemens. *Simcenter S.T.A.R.-CCM+ -User Guide*.  
[https://docs.sw.siemens.com/en-US/doc/226870983/PL20200227072959152.userGuide\\_pdf\\_2020.1?audience=external](https://docs.sw.siemens.com/en-US/doc/226870983/PL20200227072959152.userGuide_pdf_2020.1?audience=external). Accessed 15 January 2023

[12] Anderson, J., 2017, **Fundamentals of Aerodynamics Sixth Edition**, McGraw-Hill, New York. pp 64-67.

[13] Anderson, J., 2017, **Fundamentals of Aerodynamics Sixth Edition**, McGraw-Hill, New York. pp 97.

[13] Anderson, J., 2017, **Fundamentals of Aerodynamics Sixth Edition**, McGraw-Hill, New York. pp 530.

[14] Anderson, J., 2017, **Fundamentals of Aerodynamics Sixth Edition**, McGraw-Hill, New York. pp 432-437.

[15] Anderson, J., 2017, **Fundamentals of Aerodynamics Sixth Edition**, McGraw-Hill, New York. pp 354.

[16] White, F., 2016, **Fluid Mechanics Eight Edition**, McGraw-Hill, New York, pp. 459

[17] White, F., 2016, **Fluid Mechanics Eight Edition**, McGraw-Hill, New York, pp. 810

[18] White, F., 2016, **Fluid Mechanics Eight Edition**, McGraw-Hill, New York, pp. 307-313

[19] “Facilities.” Santa Clara County Model Aircraft Skypark. <https://sccmas.org/field.php>. Accessed 8 April 2023

[20] “Balloon Performance Calculator Tutorial.” *High Altitude Science*, [www.highaltitudescience.com/pages/balloon-performance-calculator](http://www.highaltitudescience.com/pages/balloon-performance-calculator). Accessed 3 July 2023.

[21] “Balloon Performance Calculator.” *Balloon Performance Calculator*, [tools.highaltitudescience.com/](http://tools.highaltitudescience.com/). Accessed 3 July 2023.

## 6. Appendix A - High Altitude Science Survey Q&A

**Question 1:** How common is it for a Balloon to land in an unretrievable location?

**Answer:** It depends on the launch location; if you have flexibility on the launch site location then you can better control the area that the balloon might land in. Overall, this is still an estimate based on current and predicted wind patterns. For the equipment that is slightly less expensive, many times it is just assumed we will not be getting it back because it may be too hard or time-consuming to retrieve depending on where it lands.

**Question 2:** How far from the launch point are companies willing to travel to attempt payload recovery? Do corporations even care to retrieve payload?

**Answer:** Some companies may be fine without recovery, some are okay with going on a two or more-hour drive, but in general it depends on the mission and the value of the payload. You may also want to look into the GPS Boomerang, a similar glider project that could help you in your design process.

**Question 3:** At what points over the lifetime of the balloon is sensor data gathered?

**Answer:** Data is mainly gathered during ascent. As for the glide phase, I recommend starting the glide control below 60,000 feet and not focusing on generating lift above 60,000 ft.

**Question 4:** How much does the potential of unfavorable landing conditions affect the use of higher quality/value measurement equipment on weather balloons?

**Answer:** In my experience, there are set missions that we plan with expensive equipment. On these missions, we go out of our way to ensure recovery because of the large cost involved if we do not get our equipment back. Unless your entire business

involves higher-end data collection, most will not use expensive equipment because of either the cost of retrieval or the low chance of recovery.

**Question 5:** How often does the orientation of the payload once it lands on the ground affect tracking its location when retrieving? (say if it lands sideways, upside down, or in a tree)

**Answer:** It is most ideal to have the GPS facing upwards during landing so that the signal is the least obstructed. You can run into trouble tracking the payload when it lands in odd positions.

**Question 6:** If you could control the landing location of the balloon, what characteristics would a favorable landing location have? Unfavorable?

Answer: Private property that you have access to is the most ideal or generally anywhere you have permission to land. Depending on the restrictions of the area, public land could get us into trouble. For smaller, less expensive payloads, most companies just have a return address on them in hopes that someone finds it and ships it back.

**Question 7:** What would be an ideal landing radius from the predicted landing point?

**Answer:** This depends on the company and what they are willing to do. The closer the payload is to the launch point is obviously most ideal but it comes down to what each company is willing to do.

**Question 8:** Would we need an additional GPS feedback system in order to ensure the landing location is known? Do you know of any other potential solutions that might be available but less favorable due to their high cost? If a weather balloon does stray from the predicted trajectory, what sensor measurement data (if any) is useful?

**Answer:** The antenna must be facing vertically or you must have it rotate vertically. For testing, you would also need to have a licensed pilot take manual control and communicate with the FAA.

**Question 9:** How much would our system need to weigh in order to be practical for your 1200g balloons and for your 1500g balloons?

**Answer:** On our website, there is a link to an extensive calculator that gives information on balloon mass, positive lift, ascent speed, and final predicted altitude.

**Question 10:** Would higher recovery rates allow them to attach more expensive but precise equipment to their balloons?

**Answer:** It would definitely incentivize the use of more expensive equipment if there were higher recovery rates.

**Question 11:** What is the ideal range that the weather balloon should travel to collect data?

**Answer:** There isn't an ideal range it just depends on the purpose of the mission. For local missions, this range could be relatively short but I have done a mission before that involved going across the continent to Africa. It really just depends on the mission.

**Question 12:** If money wasn't an issue, what is the most ideal measuring equipment that could be attached to a weather balloon for the most precise readings? How much would something like this cost?

**Answer:** Certain equipment can cost between 5-10 thousand dollars but this is more specialized equipment with specific purposes.